e^{-}–e^{+} pair production in pulsar magnetospheres

Kouichi HIROTANI

TIARA/ASIAA-NTHU, Taiwan

IPMU

December 8, 2009

Crab nebula: Composite image of X-ray [blue] and optical [red]

§1 Introduction: The γ-ray sky

Before 2008, EGRET aboard CGRO had detected six pulsars above 100 MeV.

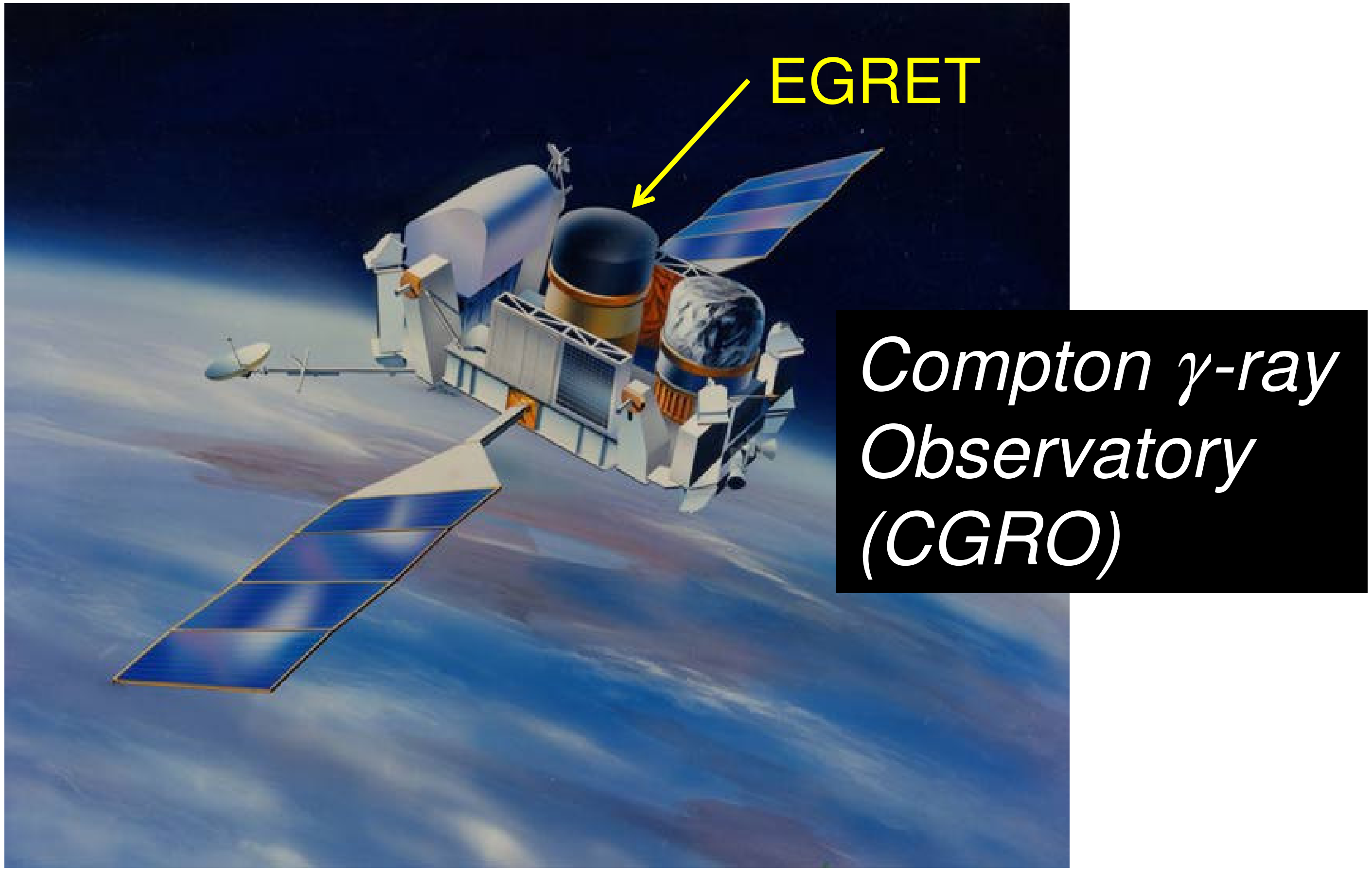

§1 Introduction: The γ-ray sky

Before 2008, EGRET aboard CGRO had detected six pulsars above 100 MeV.

EGRET point sources (>100 MeV)

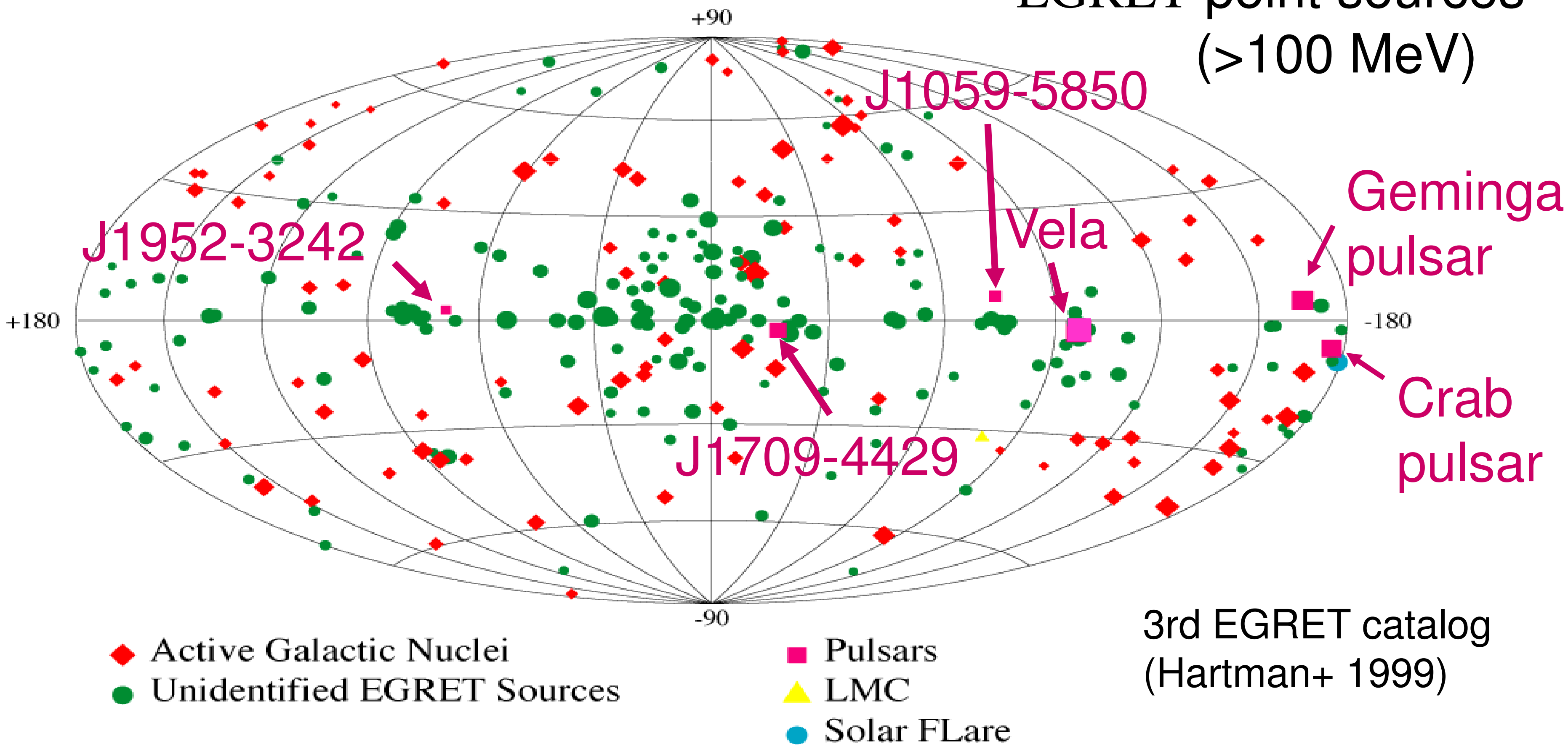

3rd EGRET catalog (Hartman+ 1999)

§1 Introduction: The γ-ray sky

After 2008, LAT aboard Fermi has detected 46 pulsars above 100 MeV.

LAT (Large Area Telescope)

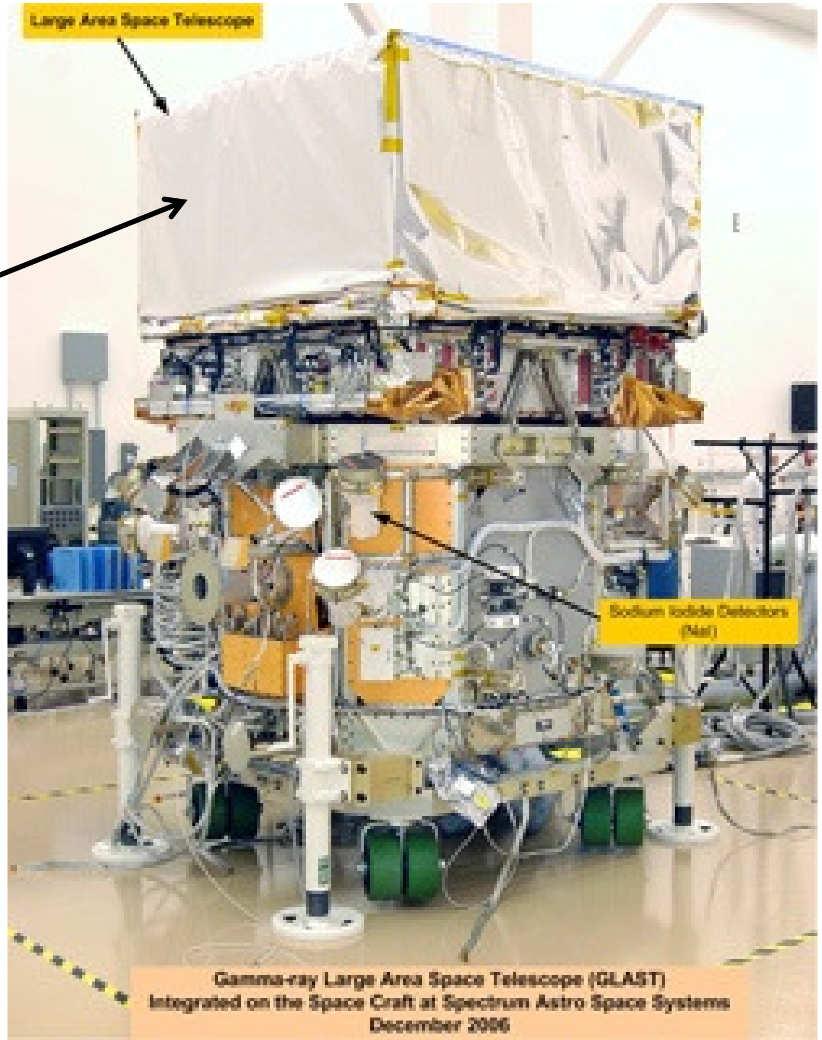

Fermi γ-ray space telescope

Launched June 2008.

§1 Introduction: The γ-ray sky

After 2008, LAT aboard Fermi has detected 46 pulsars above 100 MeV.

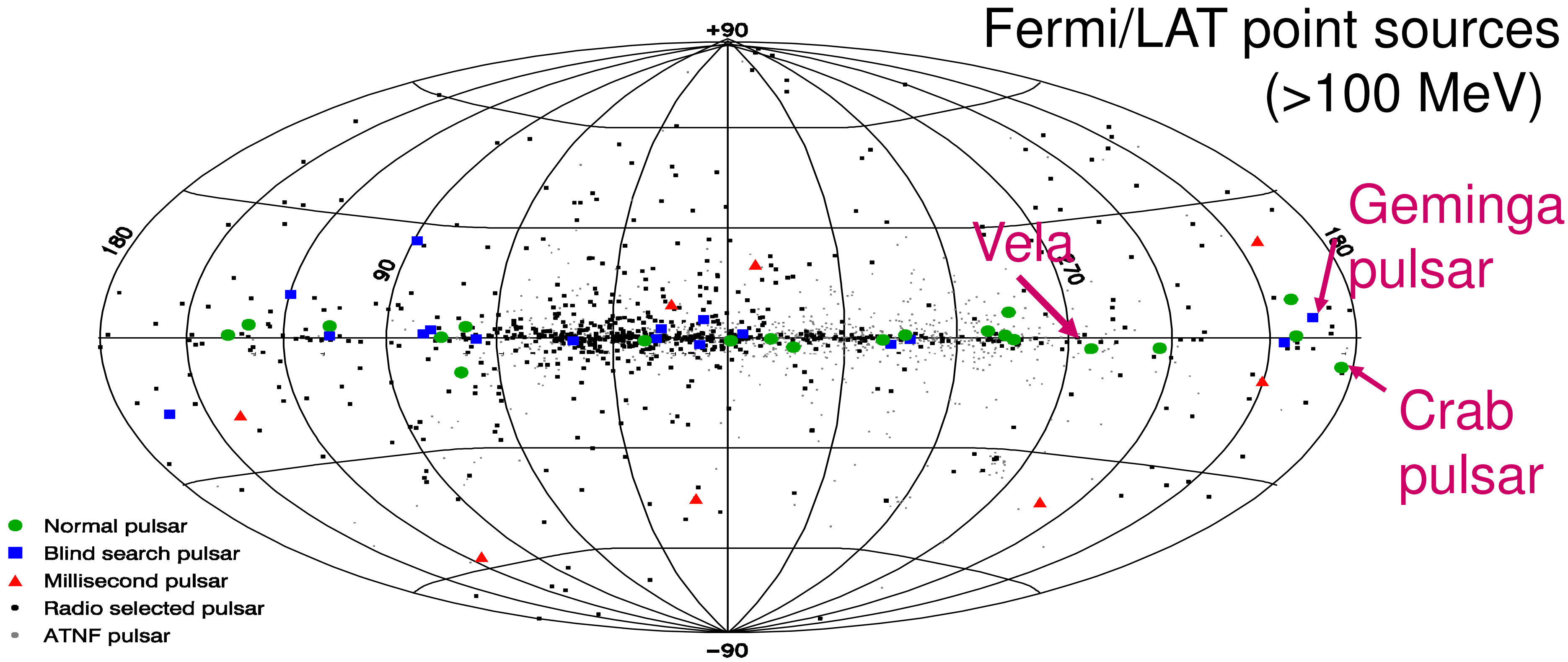

1st LAT catalog (Abdo+ 2009)

§1 Introduction: The γ-ray sky

Fermi/LAT is finding more and more nearby γ-ray pulsars.

Before Fermi, only

Geminga	250 pc
Vela	288 pc

Number increased:

2 ⟶ 6 [3:ms] (< 300 pc)

6 ⟶ 36 [8:ms] (< 5 kpc)

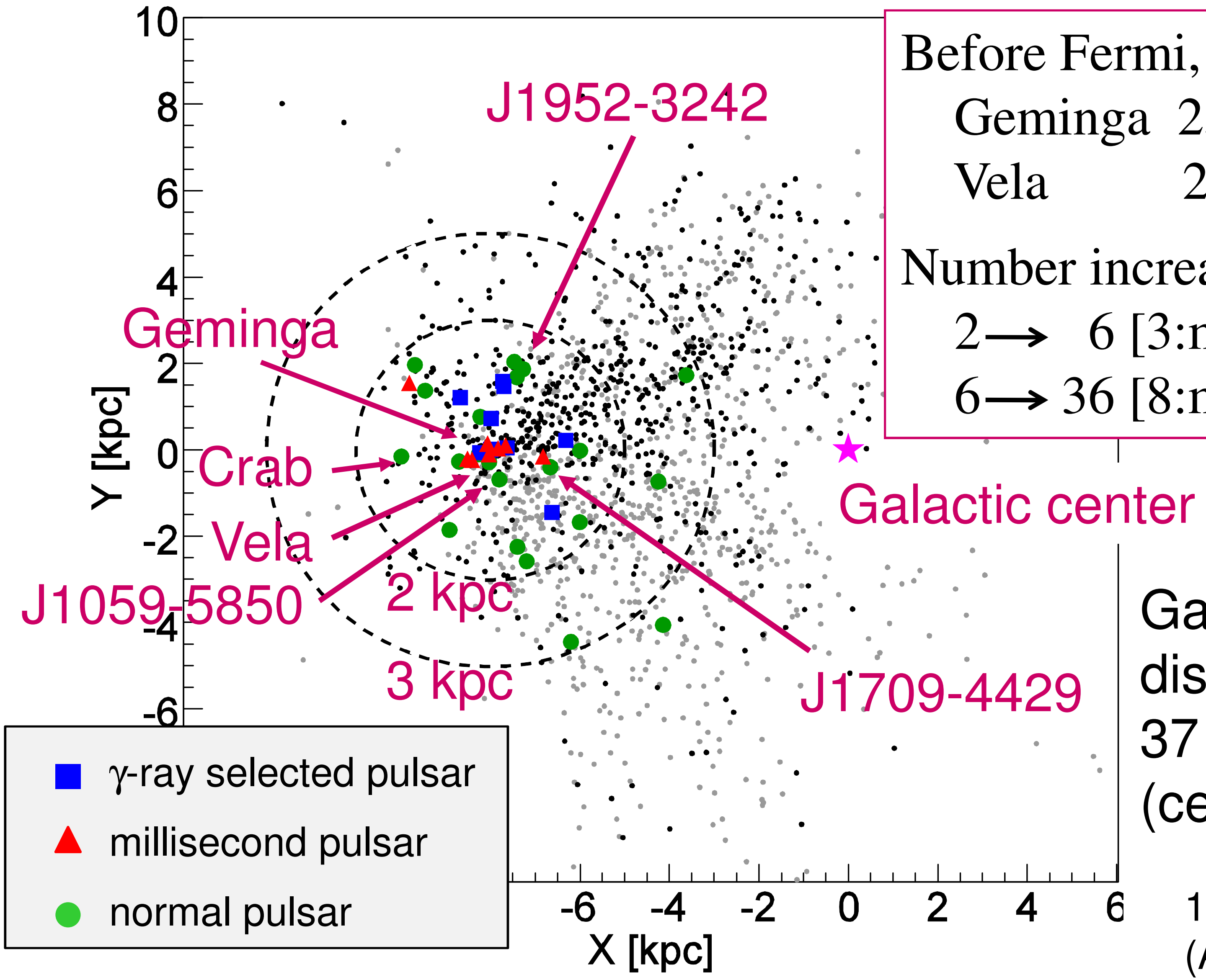

Galactic plane distribution of 37 pulsars (center: Sun)

1st LAT catalog (Abdo+ 2009)

§1 γ-ray Observations of Pulsars

Double-peak pulse profile is common.

(34 among 46 LAT pulsars)

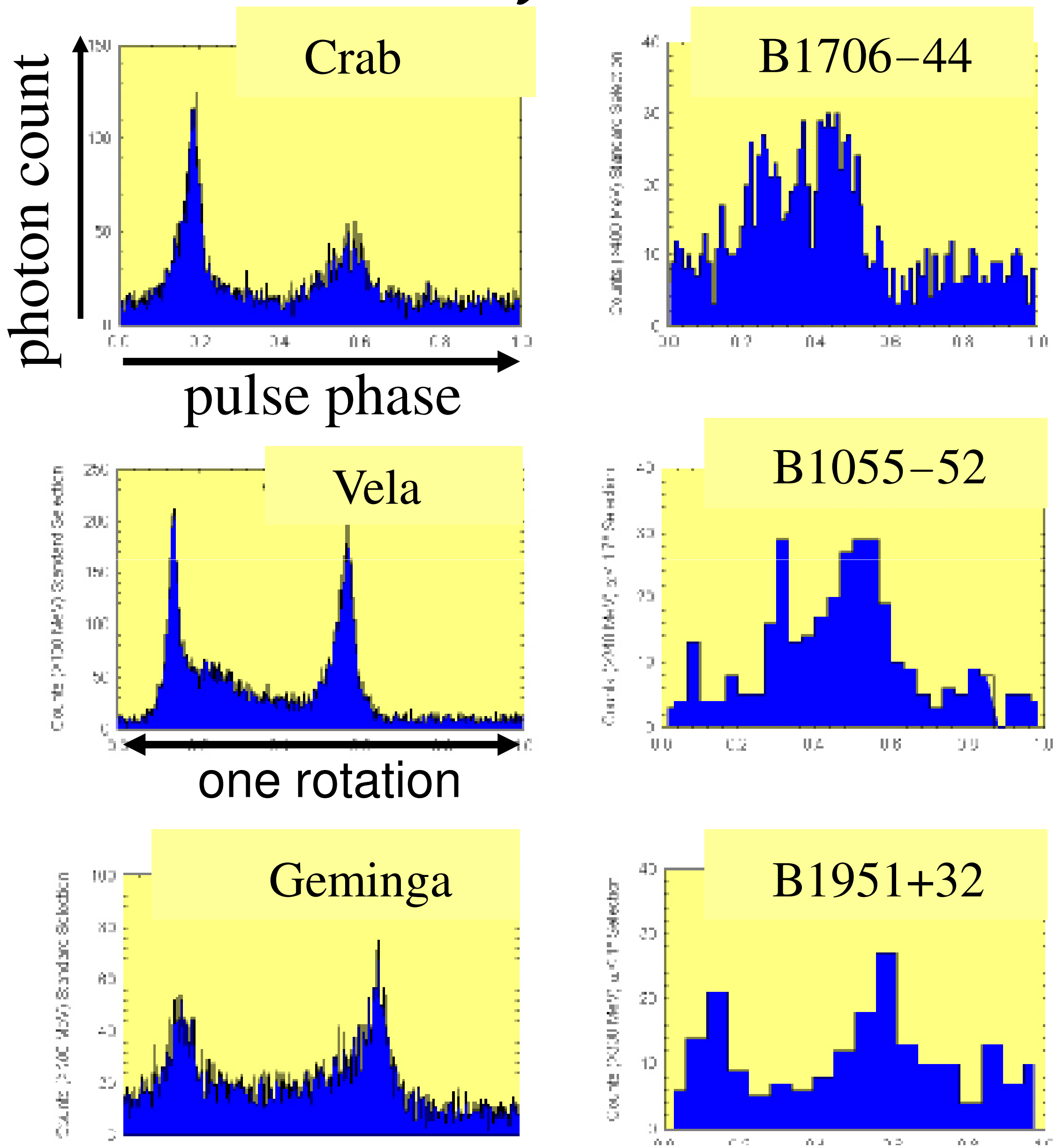

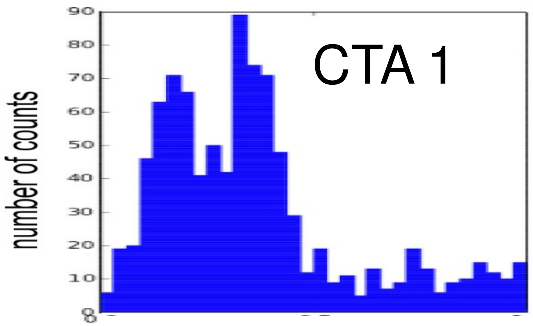

LAT (Abdo+ 08)

EGRET (Thompson 01, Kanbach 02)

§1 γ-ray Observations of Pulsars

Double-peak pulse profile is common.

(34 among 46 LAT pulsars)

Peak separation is typically between 100° and 180°.

Peak separation has no strong dependence on pulsar age (i.e., E_{spin}).

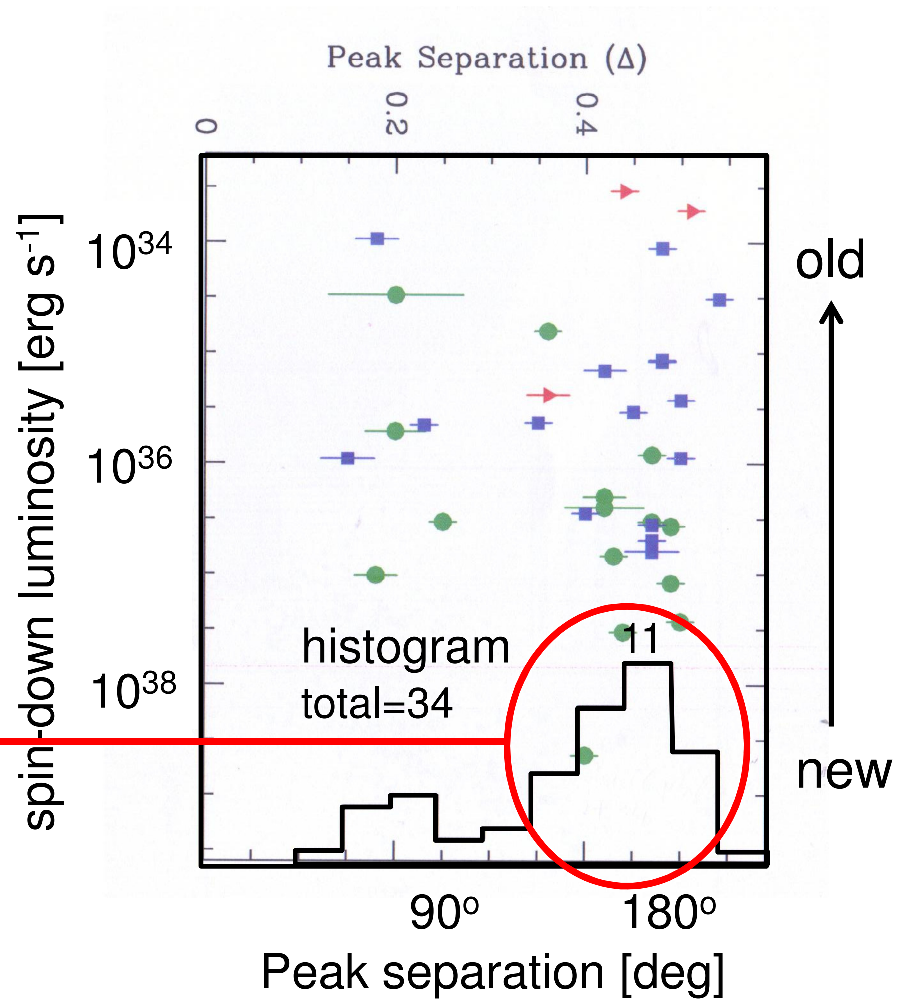

1st LAT catalog (Abdo+ 2009)

Broad-band spectra (pulsed)

- Power peaks in γ-rays
- No pulsed emission above 50 GeV
- High-energy turnover
- Spectrum gets harder as the NS ages. E.g., the **Crab** pulsar shows very soft γ-ray spectrum.
- B1951+32 shows the hardest spectrum.

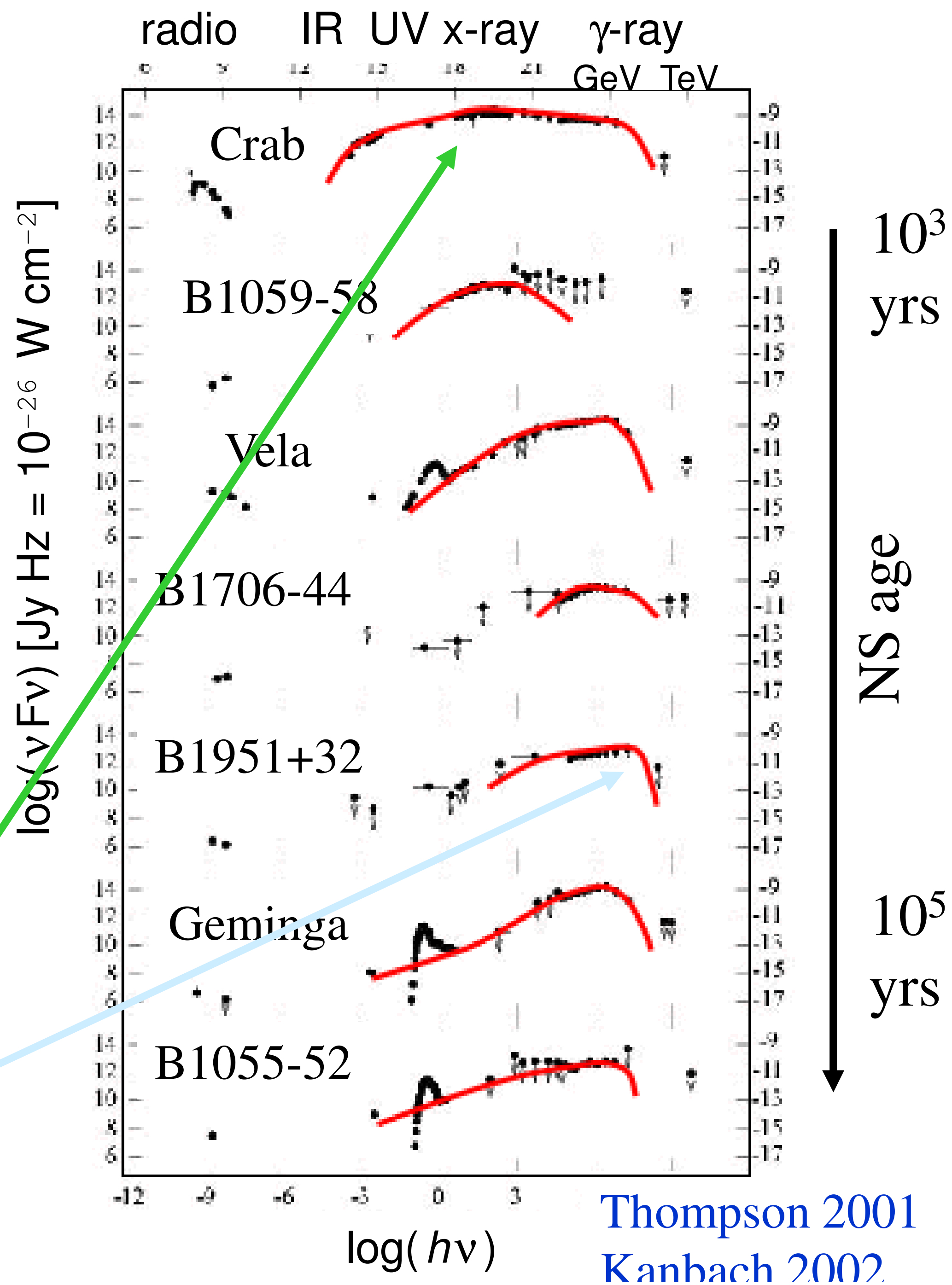

Thompson 2001
Kanbach 2002

Broad-band spectra (pulsed)

- High-energy (>100MeV) photons are emitted via **curvature** process by ultra-relativistic (~10 TeV) $e^{\pm}$'s accelerated in pulsar magnetosphere.

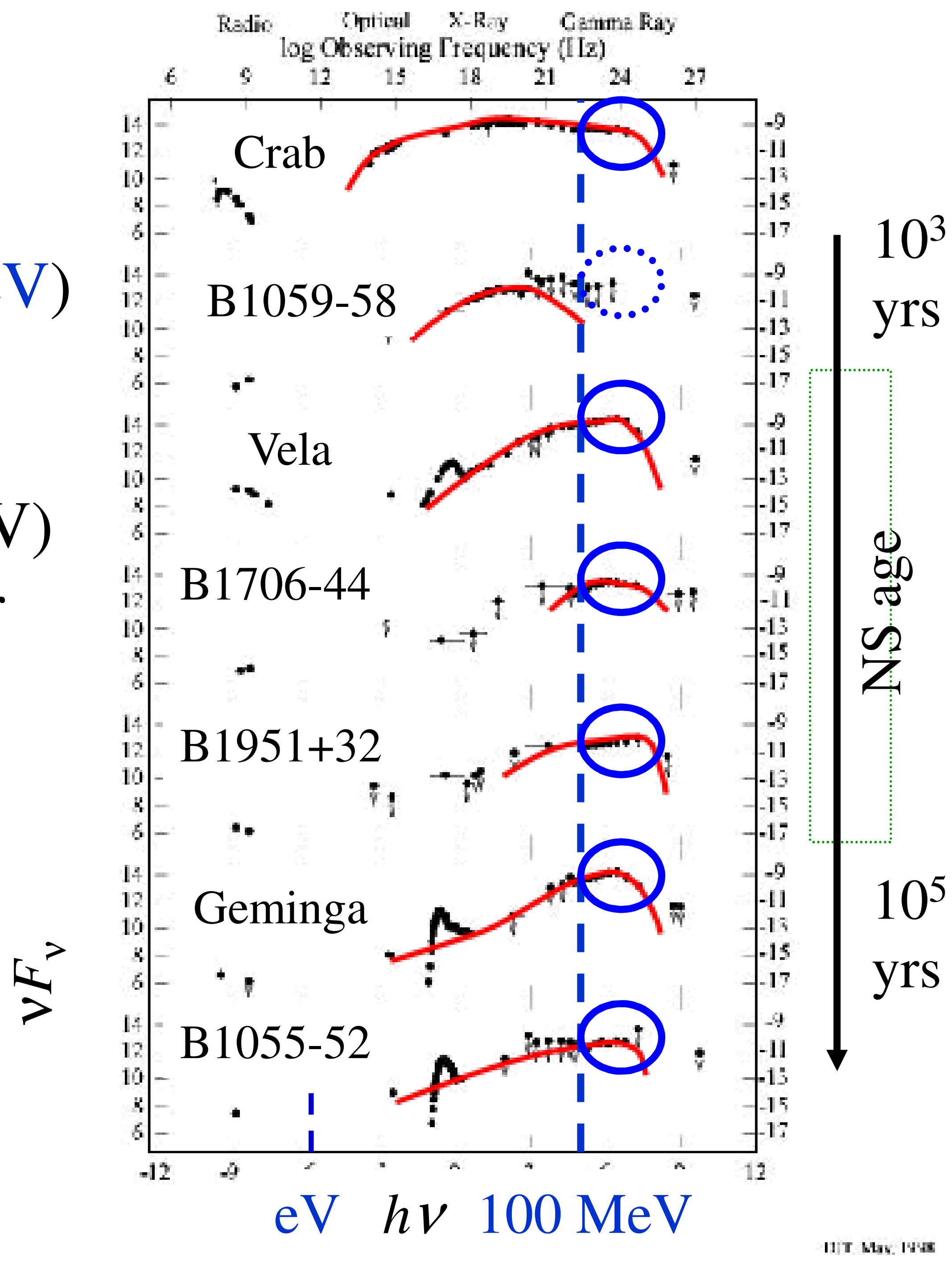

Broad-band spectra (pulsed)

- High-energy (>100MeV) photons are emitted via **curvature** process by ultra-relativistic (~10 TeV) $e^{\pm}$'s accelerated in pulsar magnetosphere.

- Some of such **primary γ-rays** are absorbed in the NS magnetosphere and reprocessed in lower energies via **synchrotron** process.

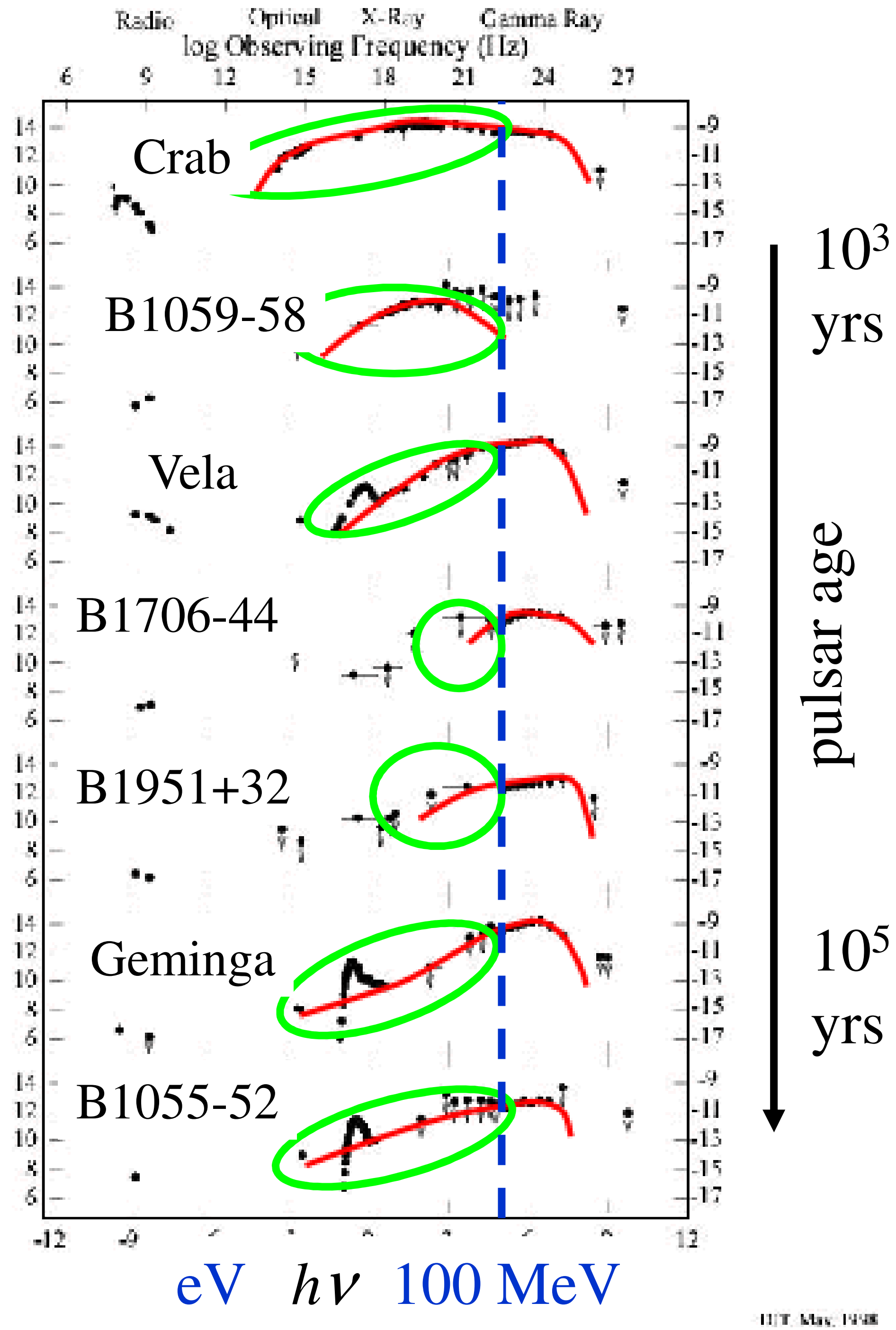

§1 Introduction

Pulsars:

rapidly rotating, highly magnetized neutrons stars (NS)

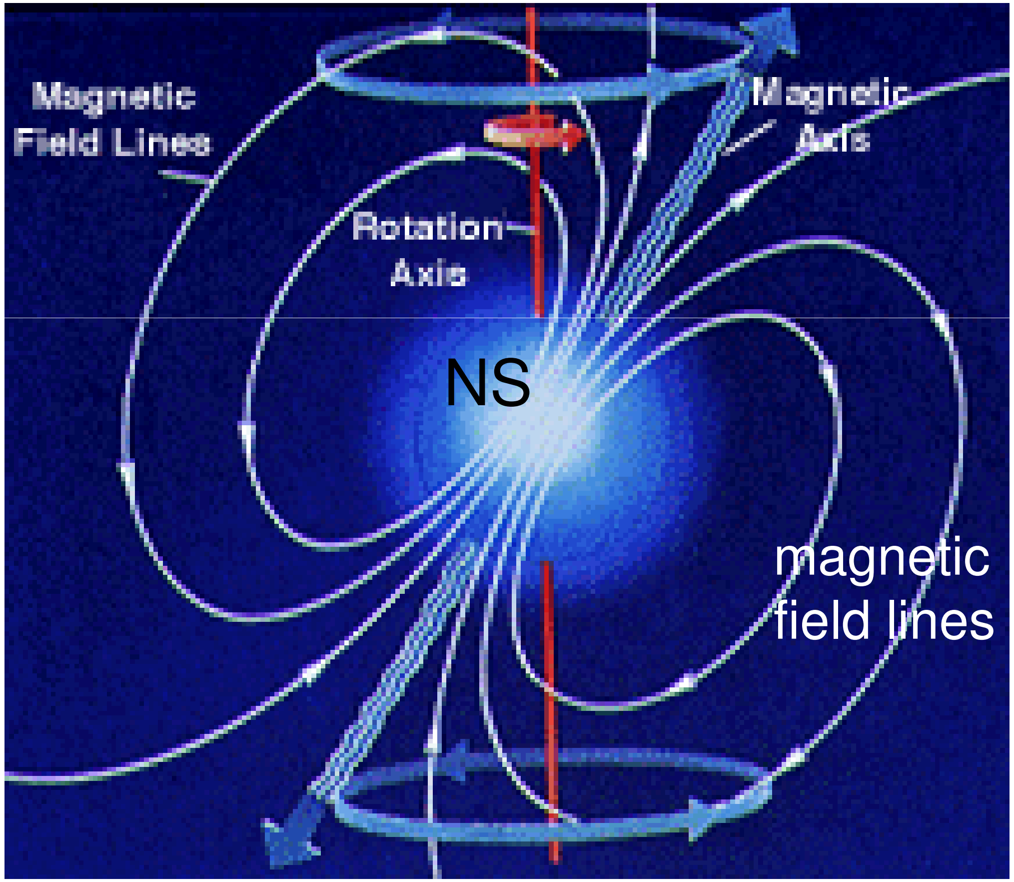

Magnetic and rotation axes are misaligned.

Pulsars turn on and off as the beam sweeps our line of sight

(e.g., lighthouse).

↓

Double-peak light curve

§1 Introduction

Pulsar emissions result from electro-dynamical extraction of NS rotational energy.

(e.g., unipolar inductor)

The rotational energy loss rate:

$$\dot{E} = I\Omega\dot{\Omega} = -(2\pi)^2 I \dot{P} P^3,$$

where $\Omega \equiv 2\pi / P$: NS rotational angular freq.,

$I \sim 10^{45}$ g cm^2: NS moment of inertia.

For typical high-energy pulsars,

$P \sim 0.1$ s, $\dot{P} \sim 10^{-13}$ s s^{-1}, give $\left|\dot{E}\right| \sim 10^{33-38.7}$ ergs s^{-1}

§1 Introduction

For such a small ($r_* \sim 10$ km) object to experience a large spin-down torque, it must have a strong coupling to their surroundings through ***B*** fields.

Spin-down luminosity: $L_{\rm spin} = k\,\Omega^4 \mu^2/c^3$.

For a dipole radiation, $k = 2\sin^2\alpha_i/3$

(α_i: ***B*** inclination angle with respect to spin axis)

Equating $L_{\rm dip}$ and $-I\Omega(d\Omega/dt)$, we can infer ***B*** moment, μ.

For $P \sim 0.1$ s and $dP/dt \sim 10^{-13}$ s s^{-1},

$\mu \sim 10^{30.5}$ G cm^3 and $B_* \sim 10^{12.7}$ G.

§1 Introduction

$L_{\rm spin}$ ($< 10^{39}$ erg s^{-1}) is dissipated at …

- Inner magnetosphere
  ($r < 3r_* \sim 30$ km)
- Outer magnetosphere
  ($r \sim 1000$ km)
- Wind region
  ($r \sim$ pc)
  80-99.9% of $L_{\rm spin}$ to be converted into $e^{\pm}$s' $E_{\rm kin}$.

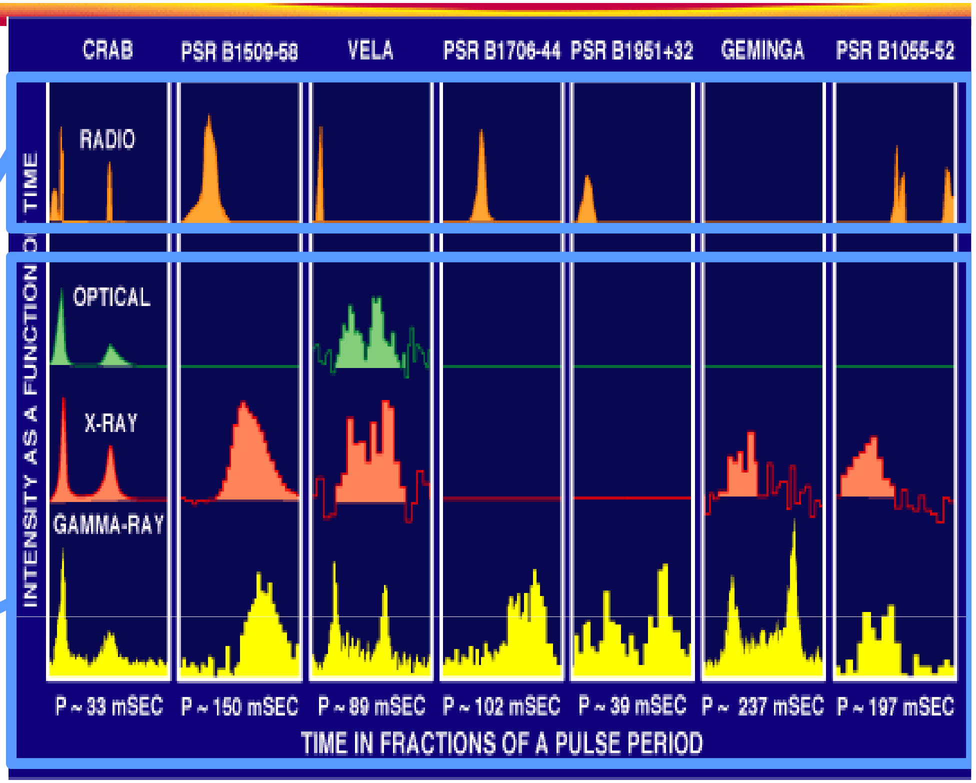

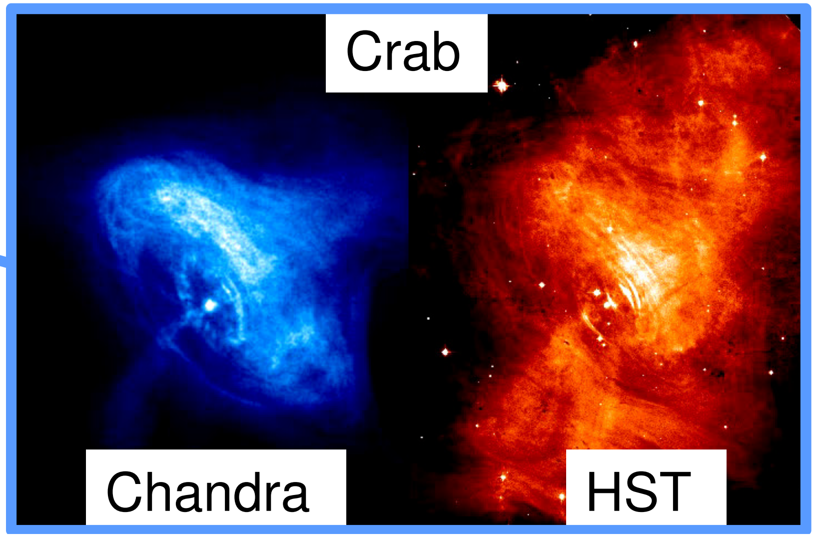

§1 Introduction

$L_{\rm spin}$ ($< 10^{39}$ erg s^{-1}) is dissipated at …

		pair energy $\gamma m_e c^2$	@ rate $e^{\pm}$'s s^{-1}
● Inner magnetosphere ($r < 3r_* \sim 30$ km)	$\sim 0.001\%$ → pulsed radio	$<$ GeV → wind $e^{\pm}$'s	$\sim 10^{40}$
● Outer magnetosphere ($r \sim 1000$ km)	0.1–20% → pulsed X, γ-ray	< 10 TeV	$\sim 10^{36}$
● Wind region ($r \sim$ pc)	99.9–80% → PWN emission re-accelerated $e^{\pm}$'s into ISM	> 10 GeV	

§1 Introduction

To interpret PAMELA and ATIC results …

		pair energy $\gamma m_e c^2$	@ rate $e^{\pm}$'s s^{-1}
● Inner magnetosphere ($r < 3r_* \sim 30$ km) → pulsed radio	~ 0.001%	< GeV	~10^{40} → wind $e^{\pm}$'s
● Outer magnetosphere ($r \sim 1000$ km) → pulsed X, γ-ray	0.1–20%	< 10 TeV	~10^{36}
● Wind region (r ~ pc) → PWN emission	99.9–80%	> 10 GeV	

re-accelerated $e^{\pm}$'s into ISM

§1 Introduction

To interpret PAMELA and ATIC results …		pair energy $\gamma m_e c^2$	@ rate $e^{\pm}$'s s^{-1}
● Inner magnetosphere ($r < 3r_* \sim 30$ km)	~ 0.001% → pulsed radio	< GeV	~10^{40} → wind $e^{\pm}$'s
● Outer magnetosphere ($r \sim 1000$ km)	0.1–20% → pulsed X, γ-ray	< 10 TeV	~10^{36}

Nevertheless, investigating a self-consistent treatment of $e^{\pm}$ creation/acceleration in pulsar magnetosphere, will help us understand an astrophysical origin of pair plasmas.

→ Consider $e^{\pm}$ creation/acceleration in outer magnetosphere.

§2 Basic Emission Mechanism

A rotating NS magnetosphere can be divided into open and closed zones.

Last-open field lines form the boundary of them.

In the open zone, $e^{\pm}$'s escape through the light cylinder as a pulsar wind.

In the closed zone, on the other hand, an $E_{||}$ would be very quickly screened by the dense plasmas.

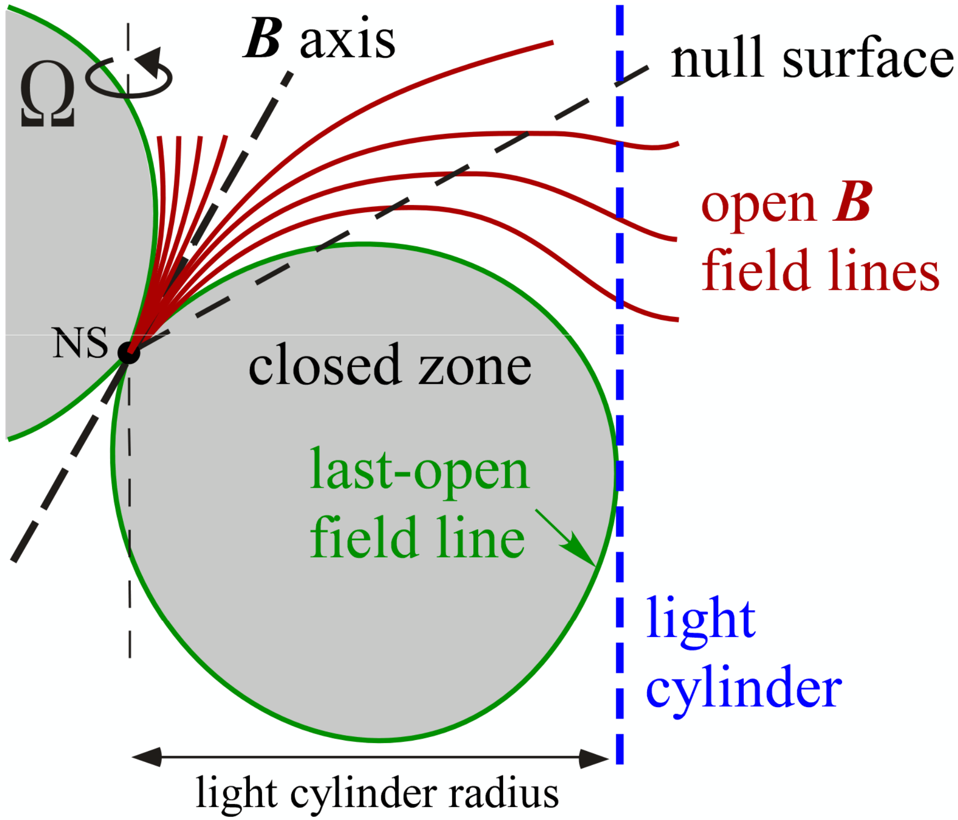

$$\varpi_{LC} = 3\times10^{8}(\Omega/10^{2}\,\mathrm{rad\,s^{-1}})\ \mathrm{cm}$$

§2 Basic Emission Mechanism

A rotating NS magnetosphere can be divided into open and closed zones.

Last-open field lines form the boundary of them.

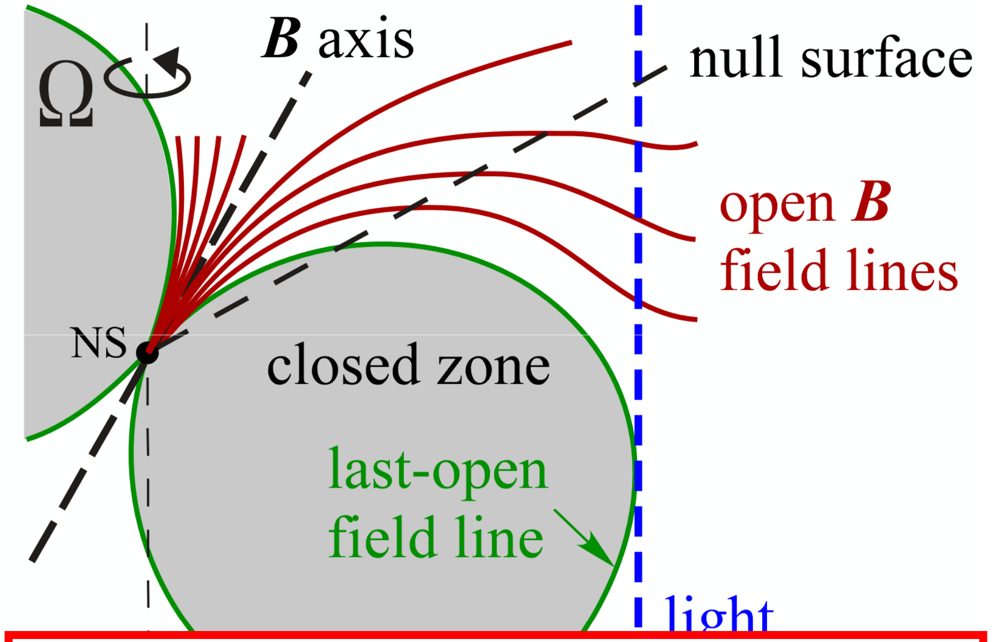

In the open zone, $e^{\pm}$'s escape through the light cylinder as a pulsar wind.

In the closed zone, on the other hand, an $E_{\parallel}$ would be very quickly screened by the dense plasmas.

Thus, in all pulsar emission models, particle acceleration takes place only within the open zone.

§2 *Basic Emission Mechanism*

For typical high-energy pulsars, open zone occupies only a few degrees from ***B*** axis on the PC surface.

Available voltage in the open zone:

$$\text{EMF} \sim \frac{\Omega^2 B_* r_*^3}{c^2} \sim 10^{15.5} \text{ V}$$

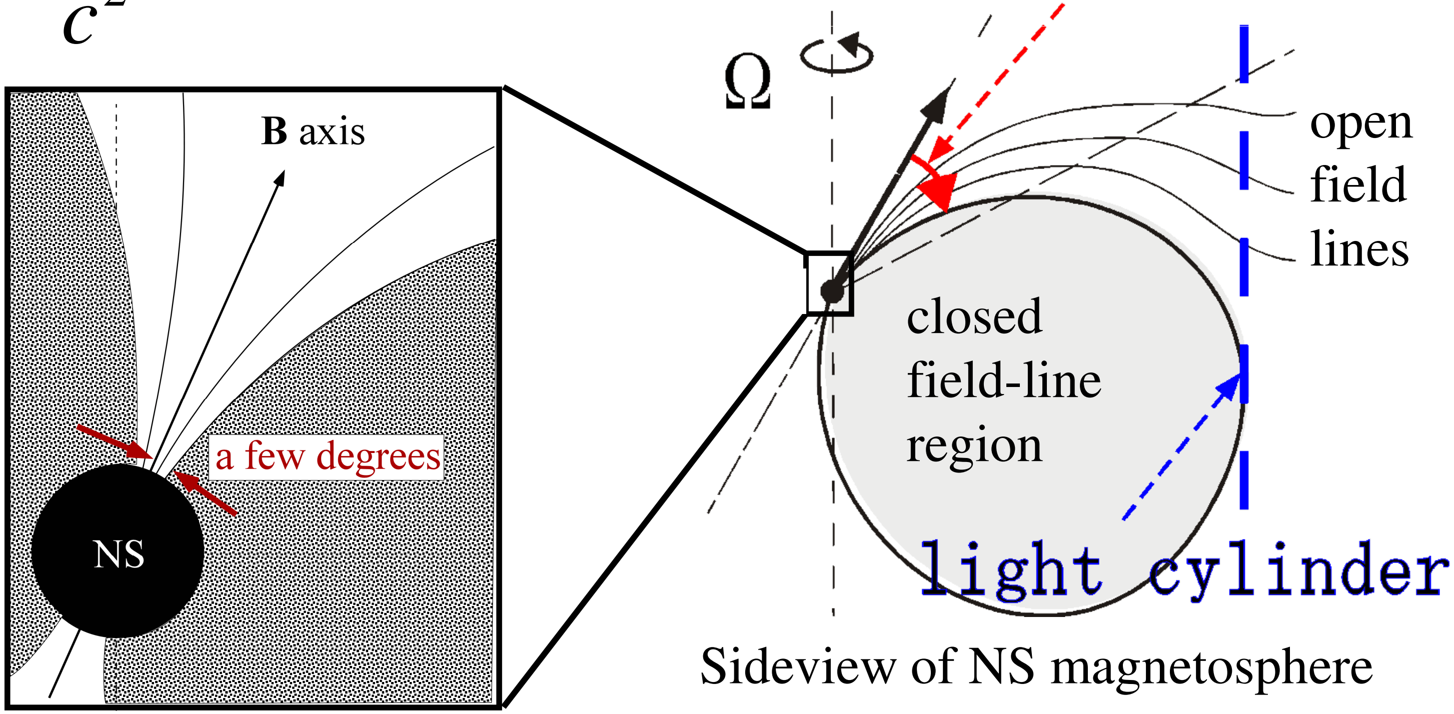

Sideview of NS magnetosphere

§2 Basic Emission Mechanism

In a rotating NS magnetosphere, the Goldreich-Julian charge density is induced for a static observer. The inhomogeneous part of Maxwell eqs. give

$$\nabla \cdot \mathbf{E}_{\parallel} = 4\pi(\rho - \rho_{\mathrm{GJ}}),$$

where $E_{\parallel} \equiv \mathbf{E} \bullet \mathbf{B}$, $\rho \equiv e(n_{+} - n_{-})$ and

$$\rho_{\mathrm{GJ}} \equiv \frac{1}{4\pi} \nabla \cdot \mathbf{E}_{\perp} = -\frac{\mathbf{\Omega} \cdot \mathbf{B}}{2\pi c}.$$

It follows that $E_{\parallel}$ arises if $\rho \neq \rho_{\mathrm{GJ}}$.

Note that ρ_{GJ} is uniquely determined by B-field geometry. For example, it changes at the so-called ‘null-charge surface’.

§2 Basic Emission Mechanism

$$\rho_{\mathrm{GJ}} \equiv \frac{1}{4\pi} \nabla \cdot \mathbf{E}_{\perp}$$

$$= -\frac{\mathbf{\Omega} \cdot \mathbf{B}}{2\pi c}.$$

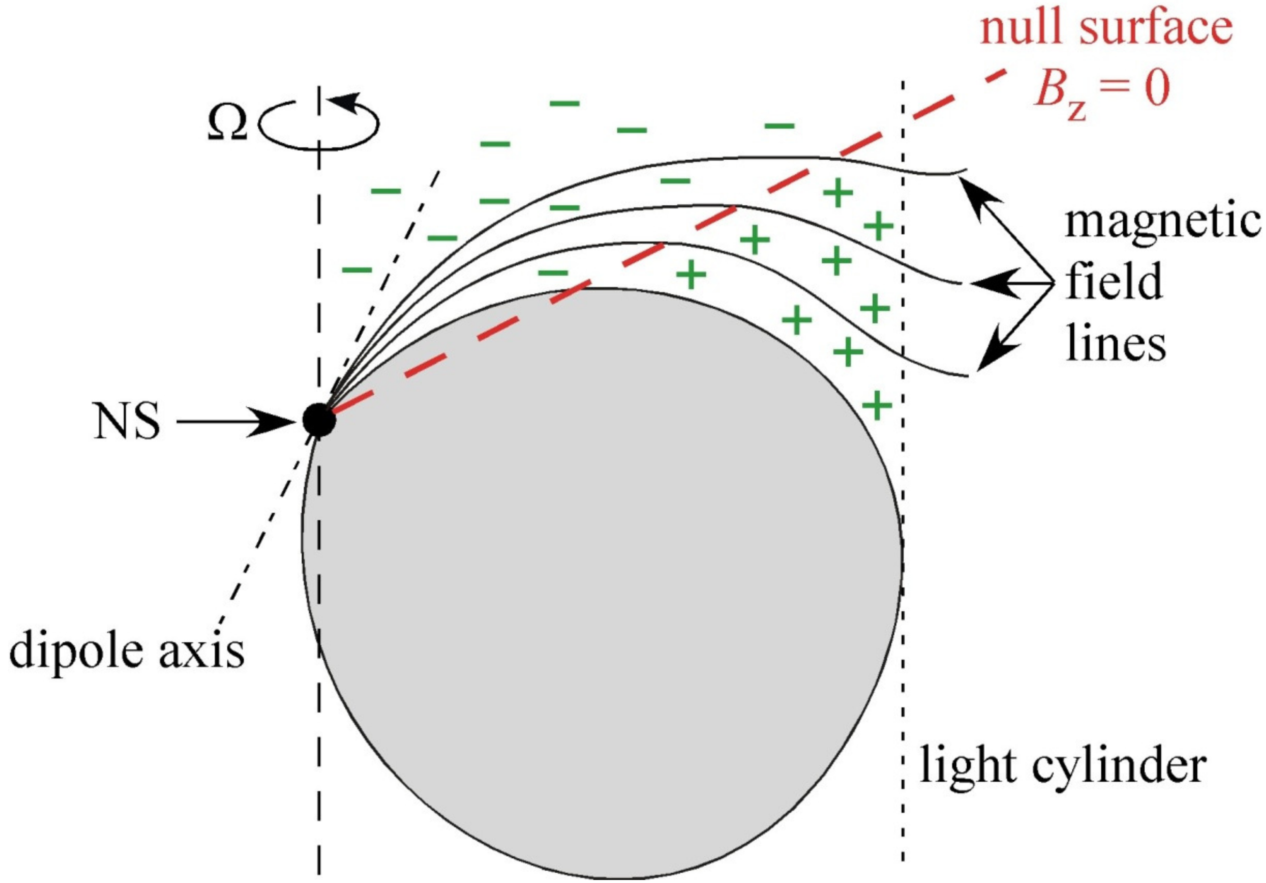

Note that ρ_{GJ} is uniquely determined by B-field geometry. For example, it changes at the so-called ‘null-charge surface’.

§3 *Emission Models*

Next question:

Where is the particle accelerator, in which $\boldsymbol{E}_{\parallel}$ arises?

In this section, we geometrically consider three representative pulsar high-energy emission models:

(historical order)

1. Inner-gap (or polar-cap) model, 1982-1990’s
2. Outer-gap model, 1986-present
3. Slot-gap model 2003-2009

Note: Inner-gap model still survives as the only theory that explains coherent radio pulsations.

§3 Emission Models

Early 80's, inner-gap model was proposed.

(Daugherty & Harding ApJ 252, 337, 1982)

Emission altitude $< 3r_{\rm NS}$ $\longrightarrow$ pencil beam ($\Delta\Omega \ll 1$ ster)

Difficult to explain wide-separated double peaks (in X-ray, γ-ray)

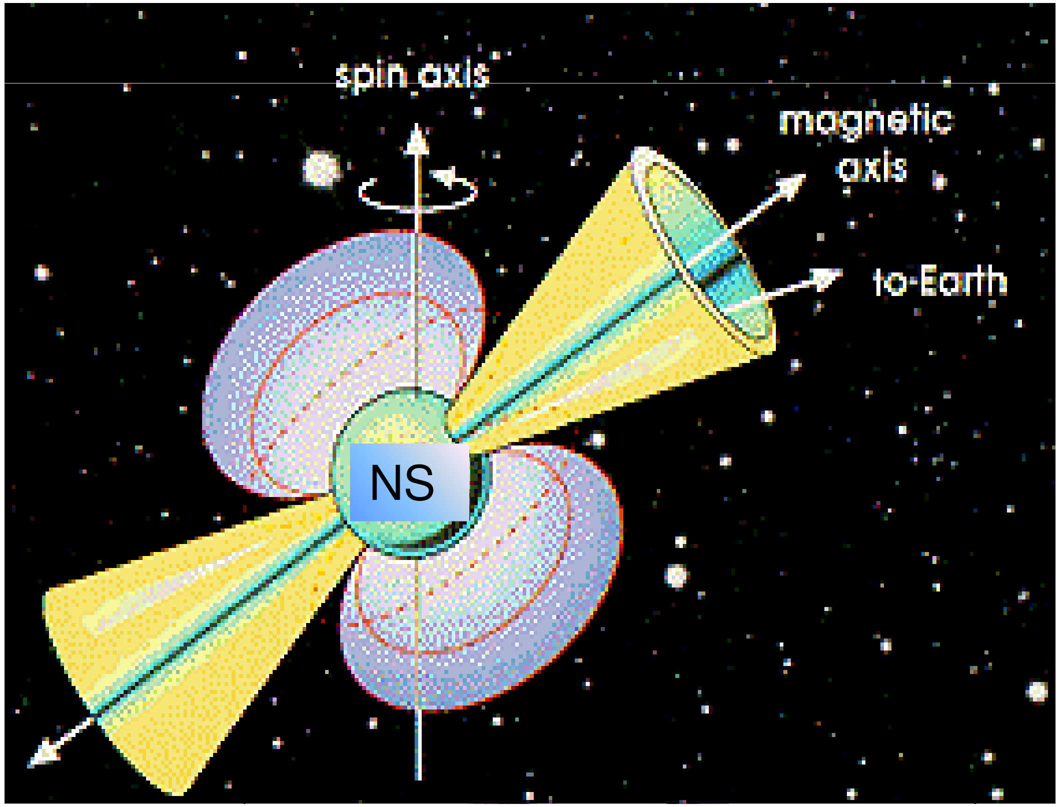

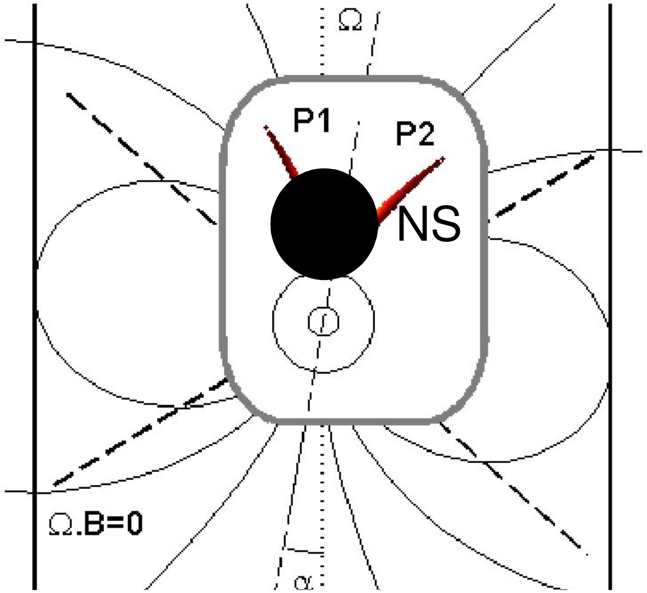

§3 *Emission Models*

Early 80's, inner-gap model was proposed.

(Daugherty & Harding ApJ 252, 337, 1982)

Emission altitude $< 3r_{\mathrm{NS}}$ $\longrightarrow$ pencil beam ($\Delta\Omega \ll 1$ ster)

Difficult to explain wide-separated double peaks (in X-ray, γ-ray)

Thus, a high-altitude emission drew attention.

§3 Emission Models

Mid 80's, outer-gap model was proposed.

(Cheng, Ho, Ruderman ApJ 300, 500, 1986)

Emission altitude > 100 r_{NS} $\longrightarrow$ hollow cone emission

($\Delta\Omega \sim 1$ ster)

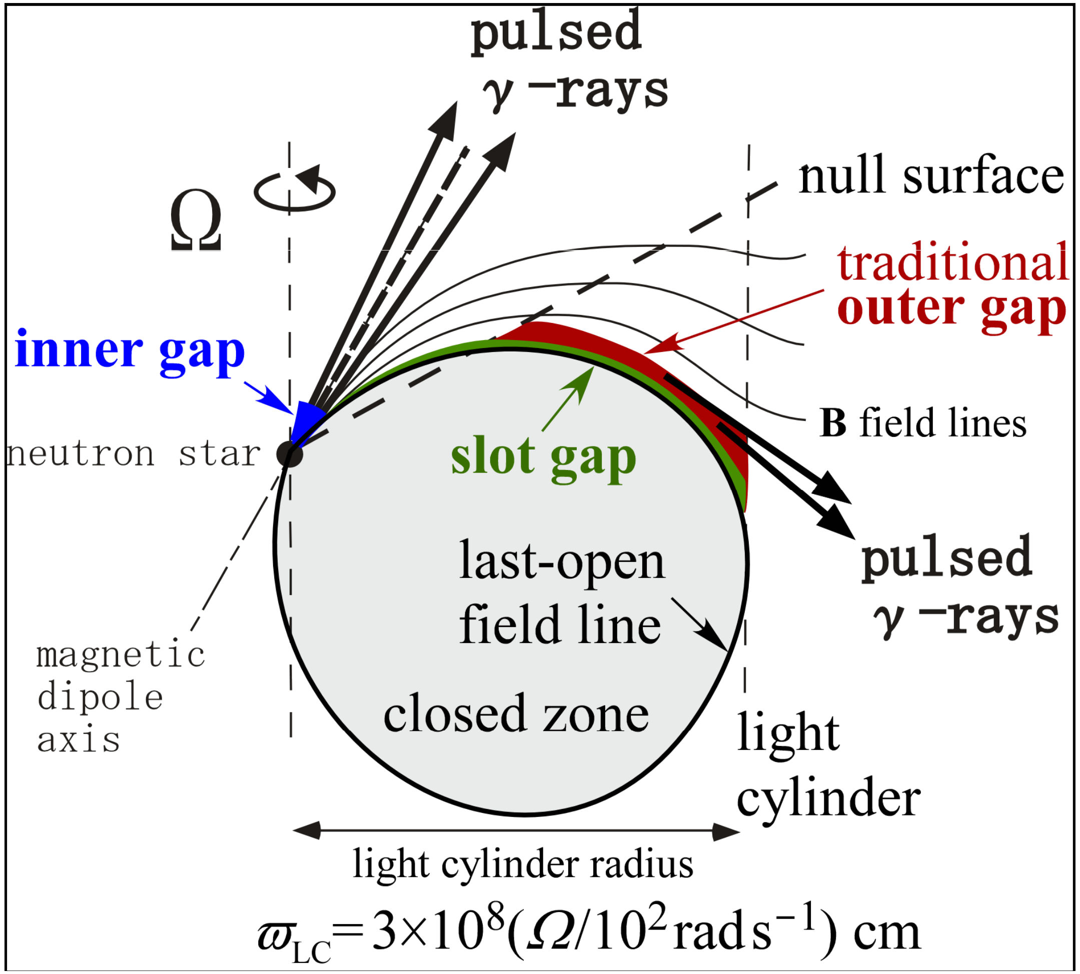

§3 Emission Models

Mid 80's, outer-gap model was proposed.

(Cheng, Ho, Ruderman ApJ 300, 500, 1986)

Emission altitude > 100 r_{NS} $\longrightarrow$ hollow cone emission

($\Delta\Omega \sim 1$ ster)

Mid 90s', the outer-gap model was further developed by taking account of special relativistic effects.

(Romani ApJ 470, 469)

$\longrightarrow$ Explains wide-separated double peaks.

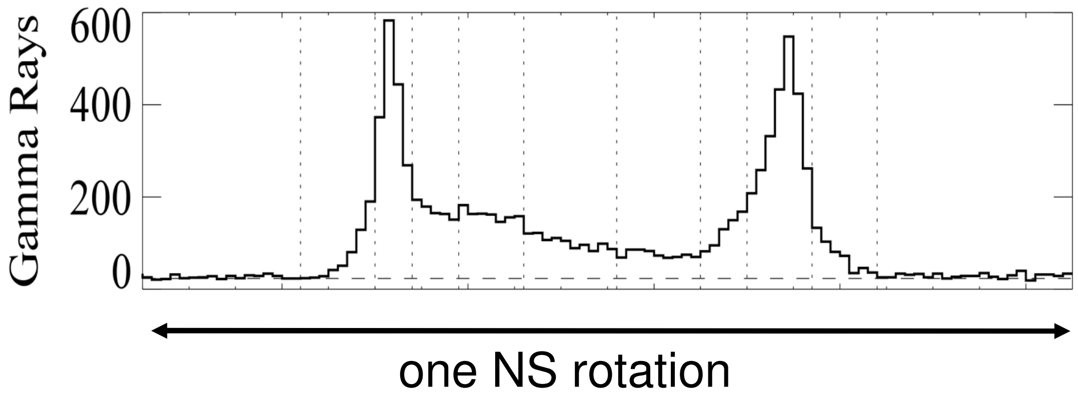

§3 Emission Models

Special relativistic effects in outer magnetosphere:

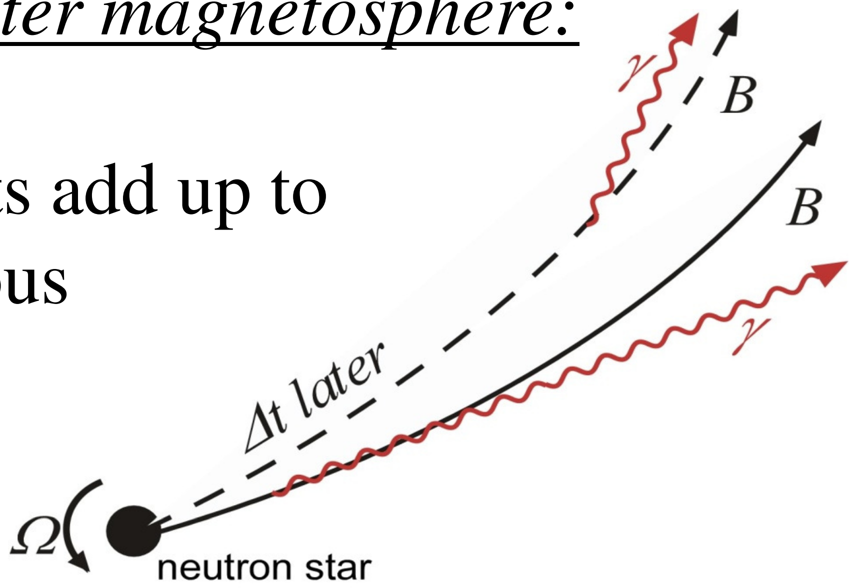

On the leading side, phase shifts add up to spread photons emitted at various altitudes over 140^o in phase.

On the trailing side, photons emitted earlier at lower altitudes catch up with those emitted later at higher altitudes to focus in a small phase range 30^o, forming caustics (strong intensity) in the phase plot.

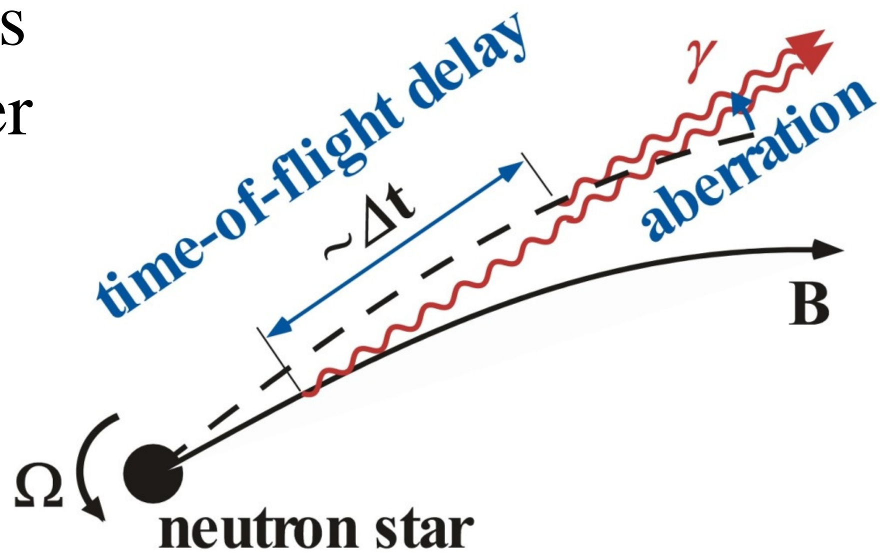

§3 *Emission Models*

Mid 80's, outer-gap model was proposed.

(Cheng, Ho, Ruderman ApJ 300, 500, 1986)

Emission altitude > 100 r_{NS} $\longrightarrow$ hollow cone emission

($\Delta\Omega \sim 1$ ster)

Mid 90s', the outer-gap model was further developed by taking account of special relativistic effects.

(Romani ApJ 470, 469)

$\longrightarrow$ Explains wide-separated double peaks.

Outer-gap model became promising.

§3 Emission Models

Early 00's, an alternative mode, slot-gap model, was proposed. (Muslimov & Harding ApJ 588, 430, 2003)

They revisited the original idea of Arons (1983), extending his lower-altitude slot-gap model into the higher altitudes (by hand).

Due to special relativistic effects, wide-separated double peaks also appear, in the same way as in the outer-gap model (although the peak formation mechanism is slightly different).

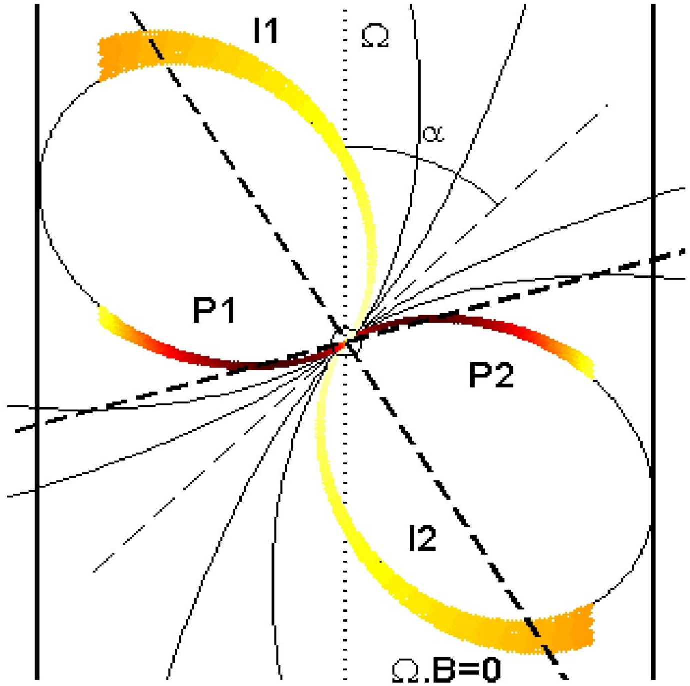

§3 Emission Models

Early 00's, two models competed:

Outer-gap model vs. Slot-gap model

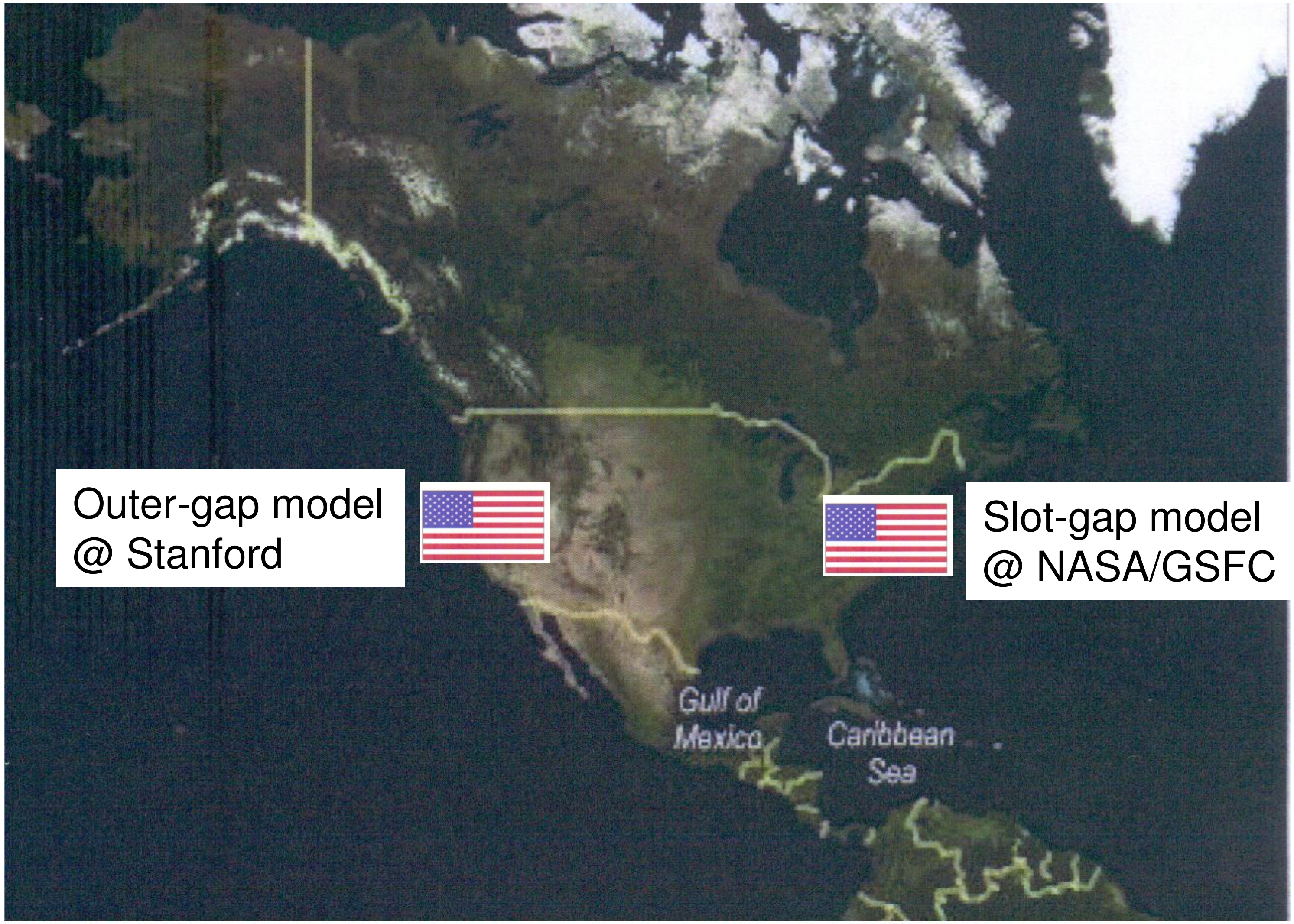

§3 Emission Models

Early 00's, two models competed:

Outer-gap model vs. Slot-gap model

A key science program of Fermi ( ):

To discriminate the two models by detailed observations.

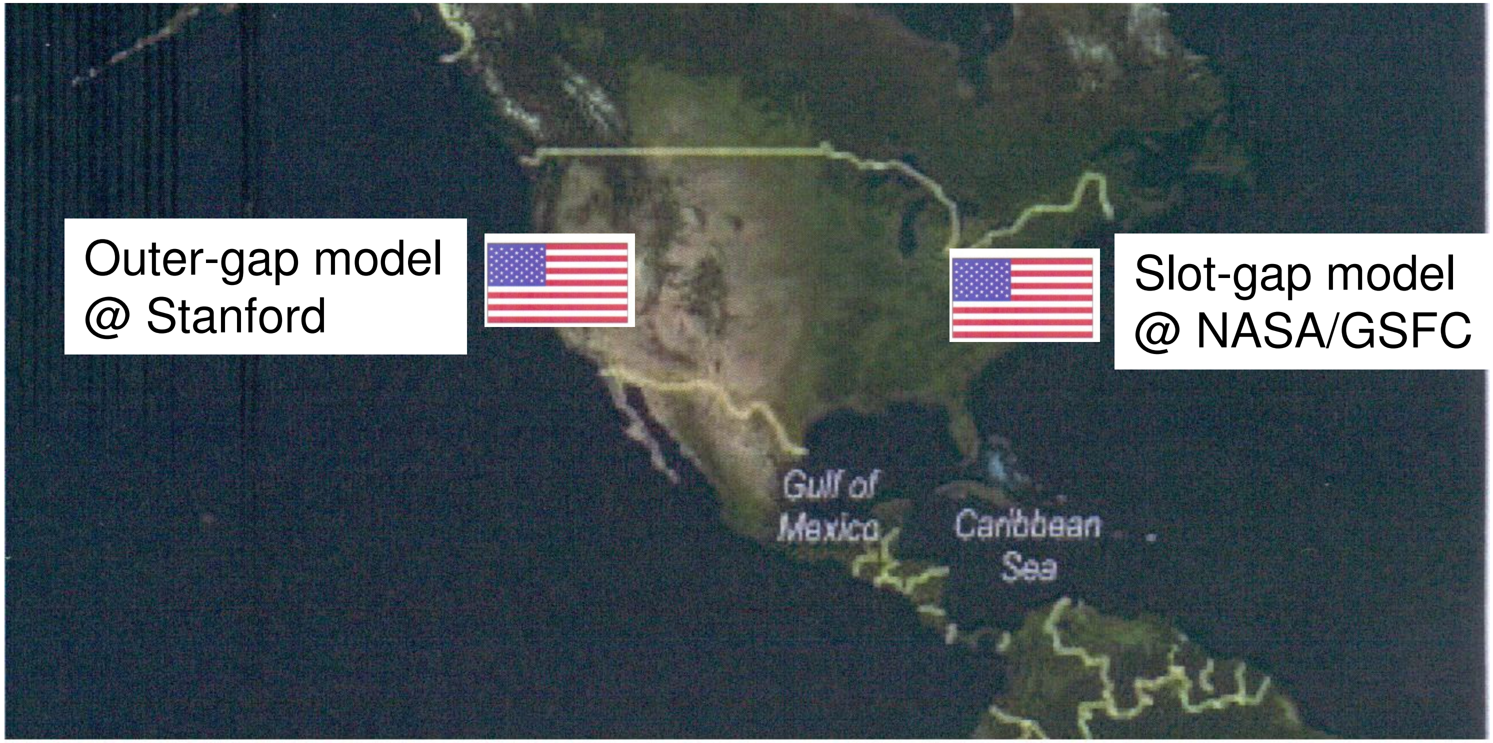

§3 Emission Models

Early 00's, two models competed:

Outer-gap model vs. Slot-gap model

A key science program of Fermi:

To discriminate the two models by detailed observations.

However, we can rule out the slot-gap model by theoretical consideration, before comparing with observations. (Hirotani ApJ 688, L25, 2008)
(Hirotani Open Astron. in press, 2009)

§4 Problems in Slot-gap model

Serious electro-dynamical problems in the SG model:

(1) Electric current closure,
(2) Unphysical assumption of the Goldreich-Julian charge density,
(3) Over-estimated electron Lorentz factors,
(4) Insufficient γ-ray luminosity

§4. Problems in Slot-gap model

(1) Current closure:

SG model (outward extension of IG model) predicts a negative $E_{\|}$ when $\mathbf{\Omega} \cdot \boldsymbol{\mu} > 0$. $E_{\|}<0$ induces an opposite gap current from the global current flow patterns.

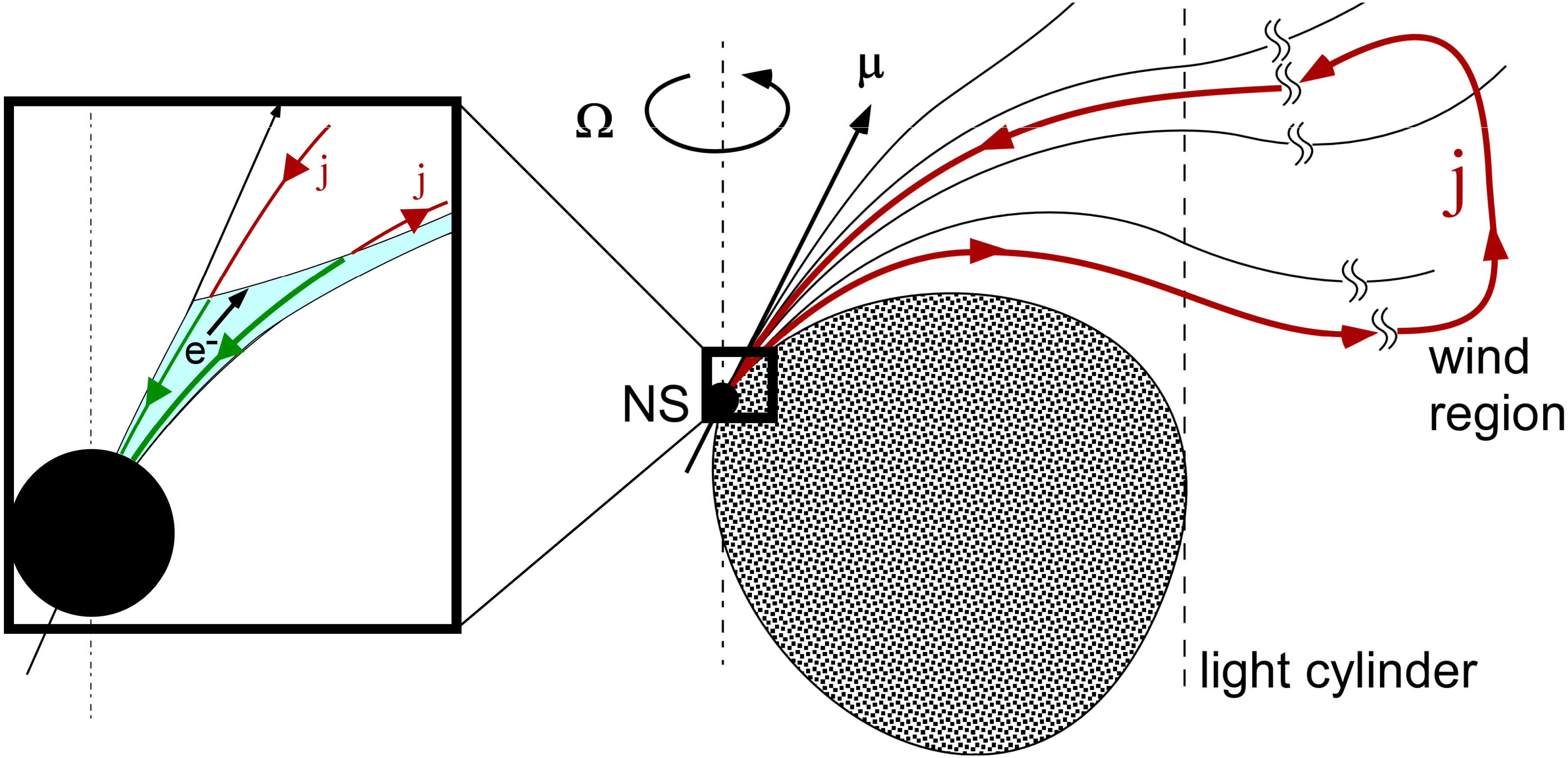

§4. Problems in Slot-gap model

(2) Artificial Goldreich-Julian charge density:

Unphysical GJ charge density is assumed in the higher altitudes.

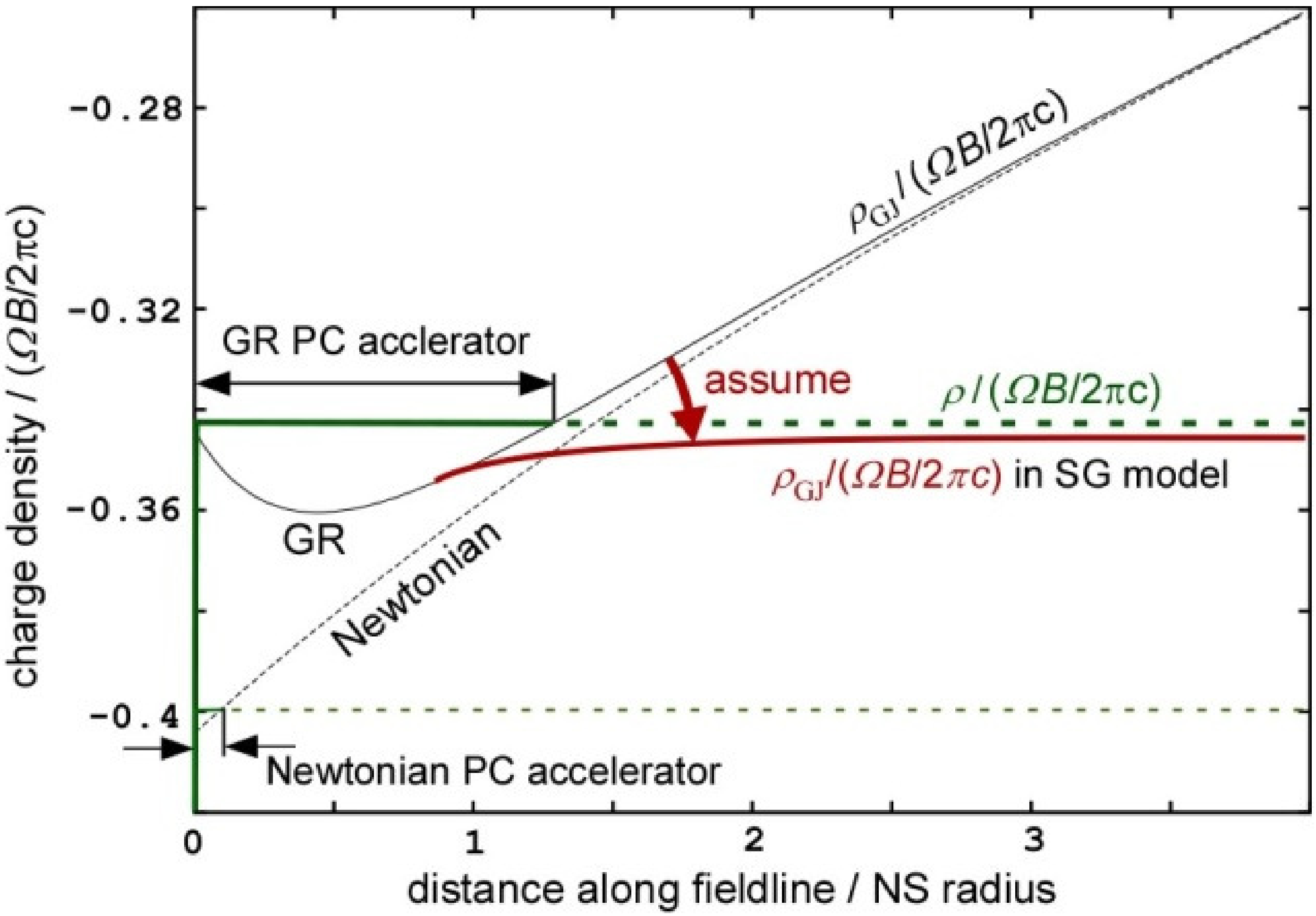

§4. Problems in Slot-gap model

(2) Artificial Goldreich-Julian charge density:

Unphysical GJ charge density is assumed in the higher altitudes. Note that $\rho_{\rm GJ}$ is geometrically determined.

$$\rho_{\rm GJ} = \frac{c^2}{4\pi\sqrt{-g}}\partial_\mu\left(\frac{\sqrt{-g}}{\rho_w^2}g^{\mu\nu}g_{\varphi\varphi}(\Omega-\omega)F_{\varphi\nu}\right).$$

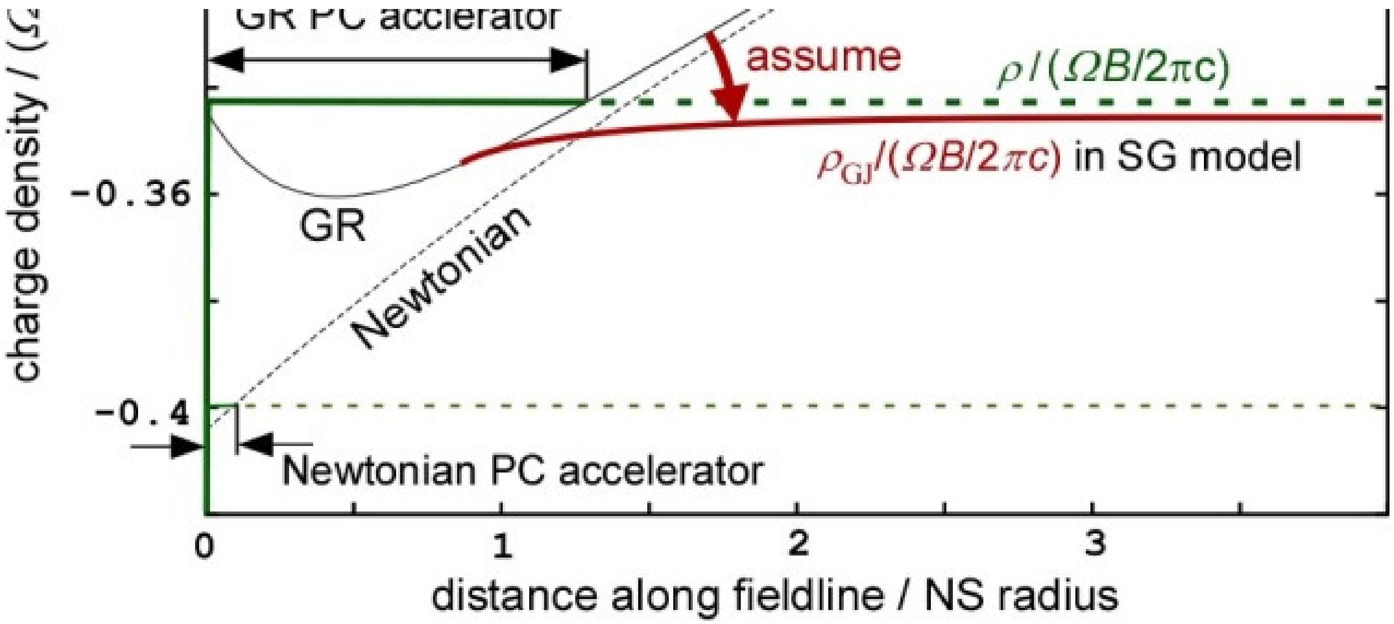

§4. Problems in Slot-gap model

(3) Systematically over-estimated electrons' Lorentz factors:

Muslimov & Harding (2003, ApJ 588, 430)

$$\Delta\Phi \approx 1.5\times10^{12}\left[1-\frac{3}{8}(1+7\delta)\right]B_{12}^{\delta}\left(\frac{I_{45}}{\lambda^8}\right)^{1/7}\mathscr{F}\ \mathrm{V}\,, \qquad (22)$$

By subs

$1.5\times10^{12}\,/\,0.5\times10^{6}$

(21) into equation (22), we ca... ...ristic Lorentz factor of primary electrons, $\gamma = e\Delta\Phi/m_e c^2$,

$$\gamma \approx \cancel{4\times10^7}\left(\frac{I_{45}}{\lambda_{0.1}^{8}}\right)^{1/7}\left[1-\frac{3}{8}(1+7\delta)\right]B_{12}^{\delta}\left(1-\frac{1}{\eta_{\rm acc}^{3}}\right)\,, \qquad (24)$$

$< 3\times10^6$

Lorentz factor: more than 13 times over-estimated.

$\longrightarrow$ L_γ is over-estimated more than 30,000 times.

§4. Problems in Slot-gap model

(3) Systematically over-estimated electrons' Lorentz factors:

Muslimov & Harding (2004, ApJ 606, 1143)

$$E_{\parallel,\mathrm{high}} \approx -\frac{3}{8}\left(\frac{\Omega R}{c}\right)^3 \frac{B_0}{f(1)} \nu_{\mathrm{SG}} \left\{ \left[1 + \frac{1}{3}\kappa\left(5 - \frac{8}{\eta_c^3}\right) + 2\frac{\eta}{\eta_{\mathrm{lc}}}\right] \right. \qquad (53)$$

$$\left. \right\}(1 - \xi_*^2). \qquad (53)$$

Terminal Lorentz factor :

$$\gamma = \left(\frac{3}{2}\frac{\rho_c{}^2}{e}E_\parallel\right)^{1/4}$$

By using equation (53) in the above equation, we arrive at

$$\gamma \sim \cancel{3 \times 10^7} \left[(2.5 + 0.6\kappa_{0.15})B_{12}\frac{R_6^3}{P_{0.1}}\frac{\eta}{\eta_{\mathrm{lc}}} \right]^{1/4} \qquad (56)$$

~1.35×10^7

L_γ is over-estimated ~ 25 times.

§4. Problems in Slot-gap model

(3) Systematically over-estimated electrons' Lorentz factors:

Harding et al. (2008, ApJ 680, 1378)

HIGH-ALTITUDE EMISSION FROM PULSAR SLOT GAPS: THE CRAB PULSAR

Received 2007 November 30; accepted 2008 March 1

~8×10^6

We present results of a 3D model of opti… ission from the slot gap accelerator of a rotation-powered pulsar. Primary electrons accelerating to high altit… …ot gap reach radiation reaction limited Lorentz factors of ~~$\sim 2\times10^7$~~, whi… …scades flow along field lines interior to the slot gap. The curvatur… …f both primary electrons and pairs produce a broad spectrum of e… …aries and pairs undergo cyclotron resonant absorption of radio p… …h angles. Synchrotron radiation from pairs with a pow… …spectrum up to ~10 MeV. Synchrotron … …eV. We examine the energy-depen… …pulsar as a function of magr… …ises, the pulse profiles are dominat… …ergy and the radio profiles, as well as the possibility … …radio cone emission. We find that the Crab pulsar profiles and spectrum can be reasonably w… …y a model with $\alpha = 45^\circ$ and $\zeta \sim 100^\circ$ or 80°. This model predicts that the slot gap emission below 2… MeV will exhibit correlations in time and phase with the radio emission.

$\Phi^{SG} = \Phi^{SG}_{low}(\eta_c) + \Phi^{SG}_{high}$ (6)

taking … and $\kappa =$ … $B_0 = $ … 0.14, $\Phi^{SG}_{tot} \simeq 1.3\times10$ …

Terminal Lorentz factor

$$\gamma = \left(\frac{3}{2}\frac{\rho_c^{\,2}}{e}E_{\parallel}\right)^{1/4}$$

L_γ is over-estimated ~ 40 times.

§4. Problems in Slot-gap model

(4) Insufficient γ-ray luminosity:

If we adopt the same parameter as Harding+('08), the predicted γ-ray flux is turned to be much less than the observed one.

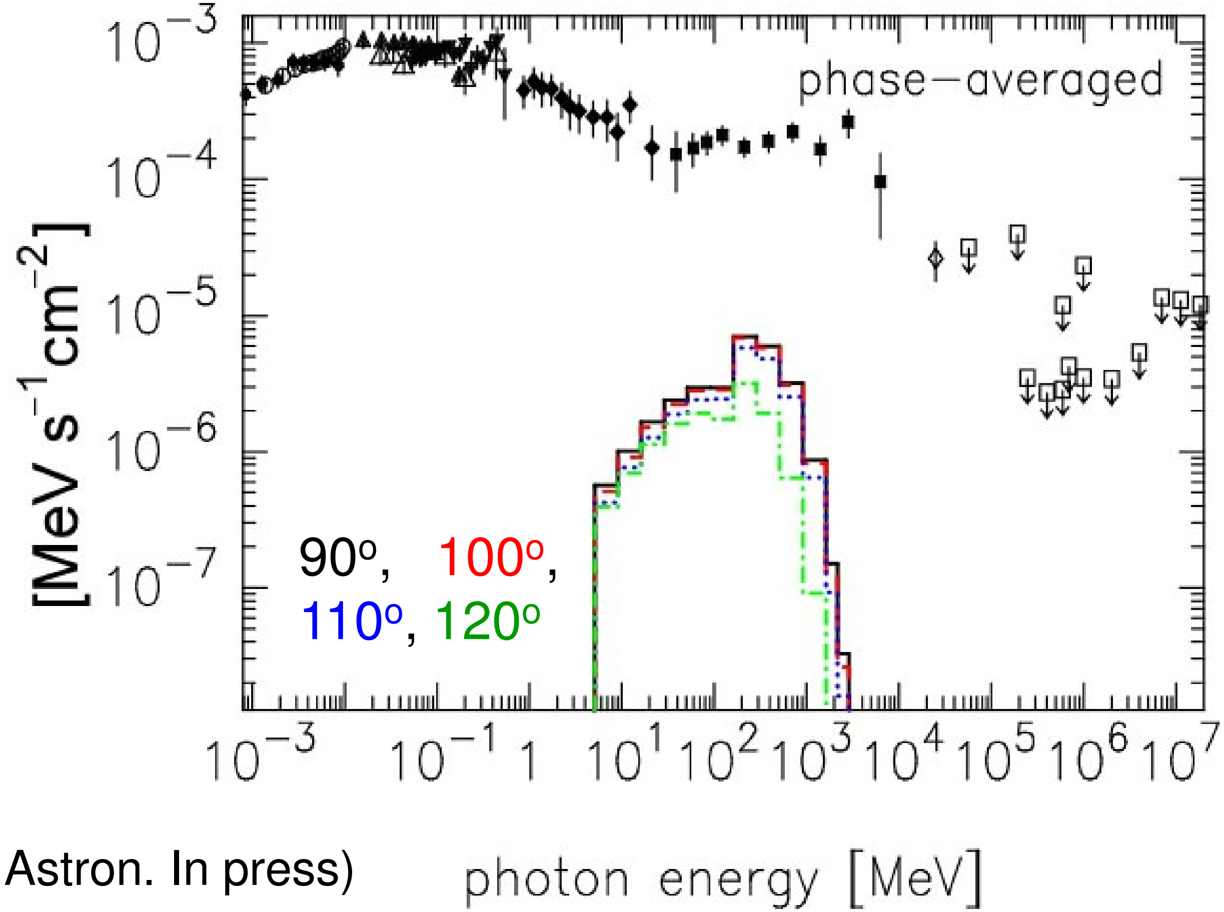

Fig. Phase-averaged SG spectrum for four discrete viewing angles, 90°, 100°, 110°, and 120°.

Hirotani (2009, Open Astron. In press)

§4. Problems in Slot-gap model

(4) Insufficient γ-ray luminosity:

SG prediction with the same parameters:

Harding + (08) Hirotani (09)

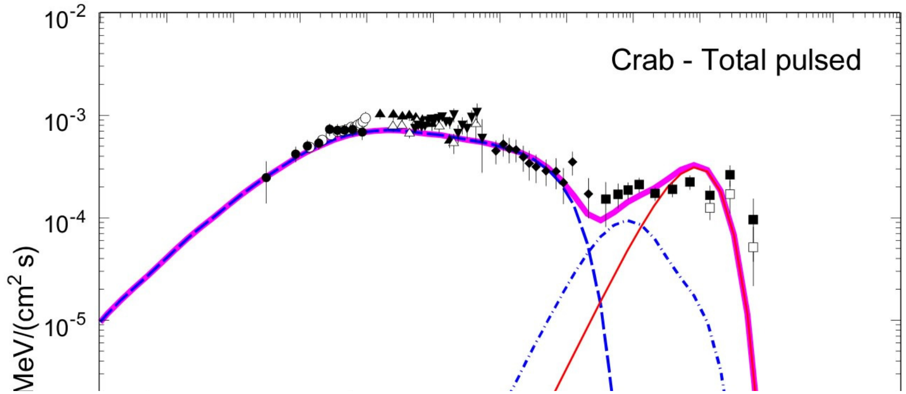

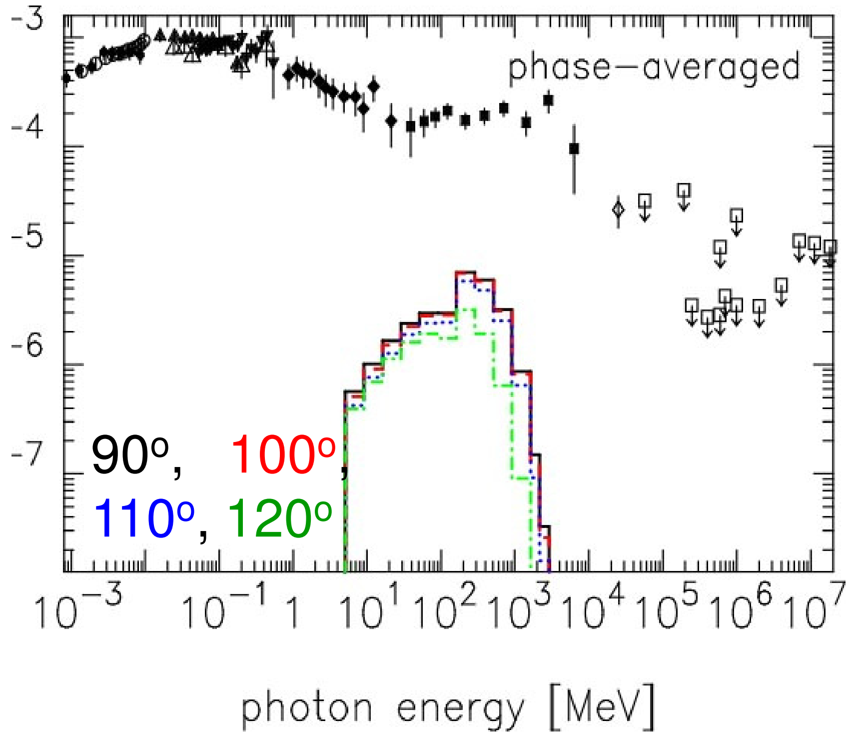

L_γ was overestimated by the overestimated Lorentz factors and, very unfortunately, by a programming bug (priv. comm)

§4. Problems in Slot-gap model

(4) Insufficient γ-ray luminosity:

The same conclusion can be obtained analytically.

(Hirotani 2008, ApJ 688, L25)

Predicted γ-ray flux of the Crab pulsar:

$$(\nu F_\nu)_{\rm peak} \approx 0.0450 f^3 \kappa \underbrace{\frac{\mu^2 \Omega^4}{c^3} \frac{1}{d^2}}_{\propto \dot{E}/d^2 \text{ : spin-down flux}}, \qquad \kappa \sim 1.$$

f : fractional gap width ($f \ll 1$ denotes a thin gap)

§4 Problems in Slot-gap model

$$(\nu F_\nu)_{\rm peak} \approx 0.0450 f^3 \kappa \frac{\mu^2 \Omega^4}{c^3} \frac{1}{d^2}$$

Apply this general result to the Crab pulsar (Ω=190 rad s^{-1}).

Hirotani (2008) ApJ 688, L25

(I) For OG model (f~0.14, κ~0.3, μ=4×10^{30} G cm^3),

$(\nu F_\nu)_{\rm peak} \sim 4\times10^{-4}$ MeV s^{-1} cm^{-2} ~ EGRET flux.

(II) For SG model (f~0.04, κ~0.2), even with a large μ,

$(\nu F_\nu)_{\rm peak} \sim 3\times10^{-5} (\mu/8 \times 10^{30})^2$ MeV s^{-1} cm^{-2}
< 0.1 EGRET flux.

OG model remains as the only possible γ-ray pulsar model.

§4 Problems in Slot-gap model

We will confirm these analytical conclusions by numerical computations in the next section.

Apply this general result to the Crab pulsar (Ω=190 rad s^{-1}).

Hirotani (2008) ApJ 688, L25

(I) For OG model (f~0.14, κ~0.3, μ=4×10^{30} G cm^3),

$$(\nu F_\nu)_{\mathrm{peak}} \sim 4\times10^{-4} \text{ MeV s}^{-1}\text{ cm}^{-2} \sim \text{EGRET flux.}$$

(II) For SG model (f~0.04, κ~0.2), even with a large μ,

$$(\nu F_\nu)_{\mathrm{peak}} \sim 3\times10^{-5}\,(\mu/8\times10^{30})^2 \text{ MeV s}^{-1}\text{ cm}^{-2}$$

$$< 0.1 \text{ EGRET flux.}$$

OG model remains as the only possible γ-ray pulsar model.

§5 New gap theory: Self-consistent approach

Stationary, self-sustained pair-production cascade in a rotating NS magnetosphere:

$e^{\pm}$'s are accelerated by $E_{||}$

Relativistic e^+/e^- emit γ-rays via synchro-curvature, and IC processes

γ-rays collide with soft photons/B to materialize as pairs in the accelerator

§5 New gap theory: Self-consistent approach

The Poisson equation for the electrostatic potential ψ is given by

$$-\nabla^2 \psi = 4\pi(\rho - \rho_{\mathrm{GJ}}) \ ,$$

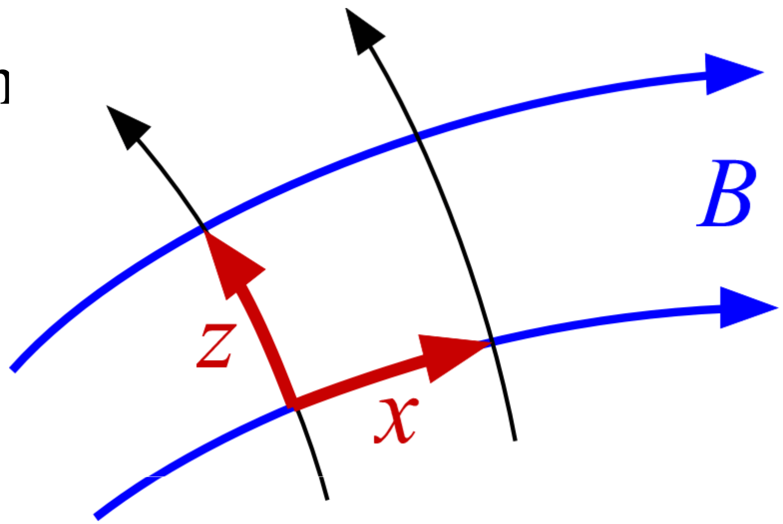

where $E_{\parallel} \equiv -\dfrac{\partial \Psi}{\partial x}$,

$$\rho \equiv e\int_0^\infty d\Gamma \left[N_+(x,z,\Gamma) - N_-(x,z,\Gamma) \right] + \rho_{\mathrm{ion}} \ ,$$

$$\rho_{\mathrm{GJ}} \equiv -\frac{\mathbf{\Omega}\bullet\mathbf{B}}{2\pi c} \ .$$

N_+/N_-: distrib. func. of e^+/e^-
Γ: Lorentz factor of e^+/e^-

§5 New gap theory: Self-consistent approach

Assuming $\partial_t + \Omega\partial_\phi = 0$, we solve the $e^\pm$'s Boltzmann eqs.

$$\frac{\partial N_\pm}{\partial t} + \vec{v}\cdot\nabla N_\pm + \left(e\vec{E}_\parallel + \frac{\vec{v}}{c}\times\vec{B} \right)\cdot\frac{\partial N_\pm}{\partial \vec{p}} = S_{IC} + \int \alpha_\nu d\nu \int \frac{I_\nu}{h\nu} d\omega$$

together with the radiative transfer equation,

$$\frac{dI_\nu}{dl} = -\alpha_\nu I_\nu + j_\nu$$

$N_\pm$: positronic/electronic spatial # density,
$E_\parallel$: mangnetic-field-aligned electric field,
S_{IC}: ICS re-distribution function, $d\omega$: solid angle element,
I_ν: specific intensity, l : path length along the ray
α_ν: absorption coefficient, j_ν: emission coefficient

§5 New gap theory: Self-consistent approach

Specify the three parameters: (period, P, is known.)

- magnetic inclination (e.g., $\alpha_{\rm inc}$=45°, 75°),
- magnetic dipole moment of NS (e.g., $\mu=4\times10^{30}\,{\rm G\,cm^3}$)
- neutron-star surface temperature (e.g., $kT_{\rm NS}$=50 eV)

Solve Poisson eq. + Boltzmann eqs. in 6-D phase space (i.e., 3-D config. + 3-D mom. space) + RTE.

I first solved (Hirotani '08, Open Astron., in press)

- gap geometry,
- acceleration electric field distribution,
- particle density and energy spectrum,
- γ-ray flux and energy spectrum,

by specifying these three parameters.

§5 New gap theory: Self-consistent approach

I applied the theory to the Crab pulsar.

§5 New gap theory: Self-consistent approach

3-D distribution of the particle accelerator (i.e., high-energy emission zone) is solved from the Poisson eq.

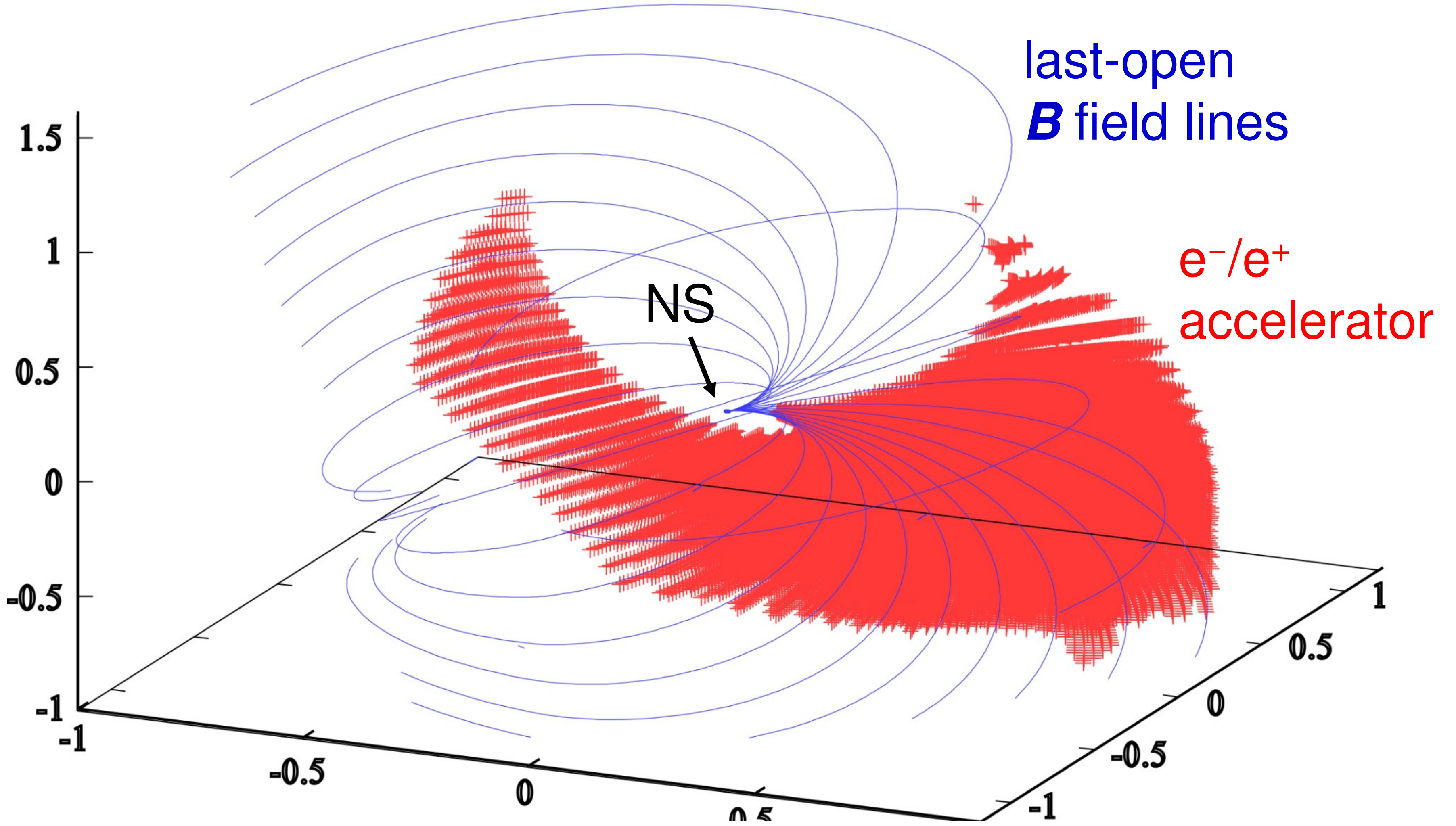

§5 New gap theory: Self-consistent approach

The gap activity is controlled by f^3.

meridional thickness, $f = f(s, \phi)$. [ϕ: magnetic azimuth]

- Previous models: assume or estimate f by dim. analysis.
- This work: solve f from the basic eqs. in 3-D mag. sphere.

Fig.) gap trans-field thickness on 2-D last-open-field-line surface

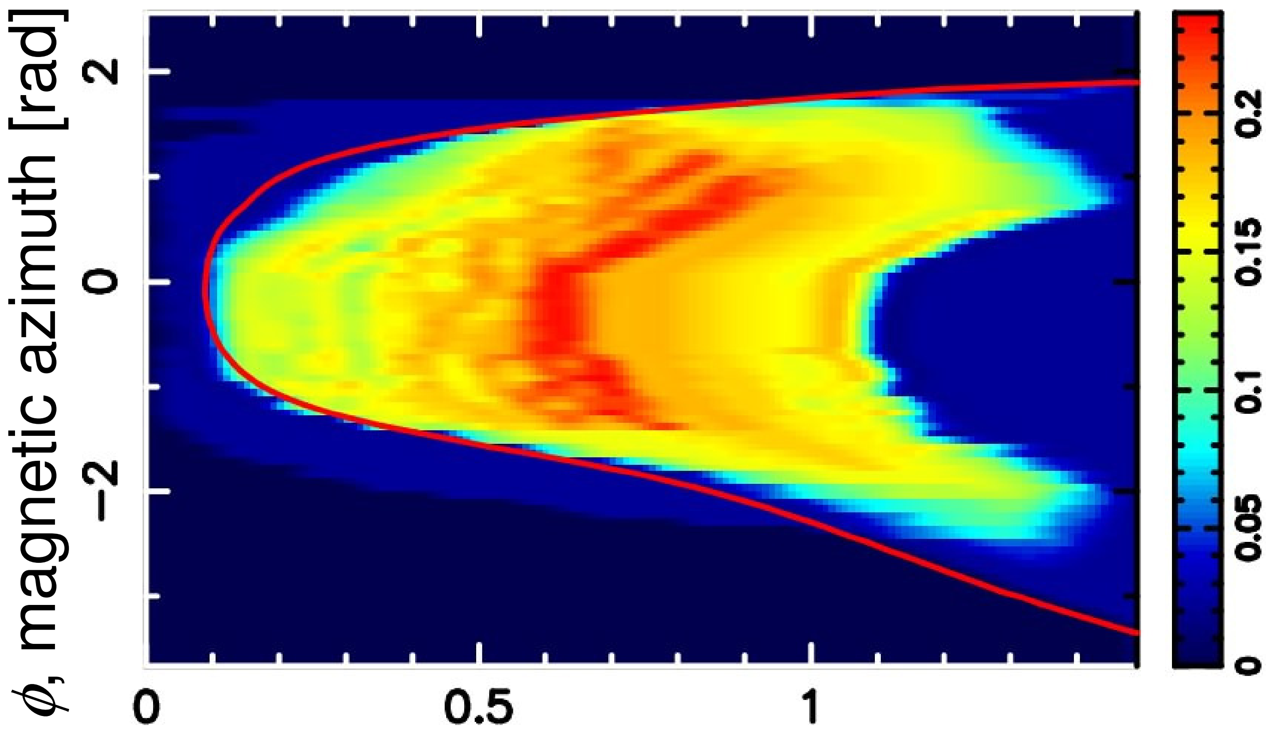

s, distance along field line / light cylinder rad.

§5 New gap theory: Self-consistent approach

Intrinsic quantities (e.g., gap 3-D geometry, f, $E_{||}$, $e^{\pm}$ distribution functions, specific intensity at each point) of an OG is self-consistently solved if we give ***B*** inclination, NS magnetic moment, NS surface temperature, without introducing any artificial assumptions.

If we additionally give the distance and observer's viewing angle, we can predict the luminosity, pulse profiles, and the photon spectrum in each pulse phase.

§5 New gap theory: Self-consistent approach

Photons are emitted along the local ***B*** field lines (in the co-rotating frame) by relativistic beaming and propagate in a hollow cone.

The hollow cone emission is projected on the 2-D propagation directional plane.

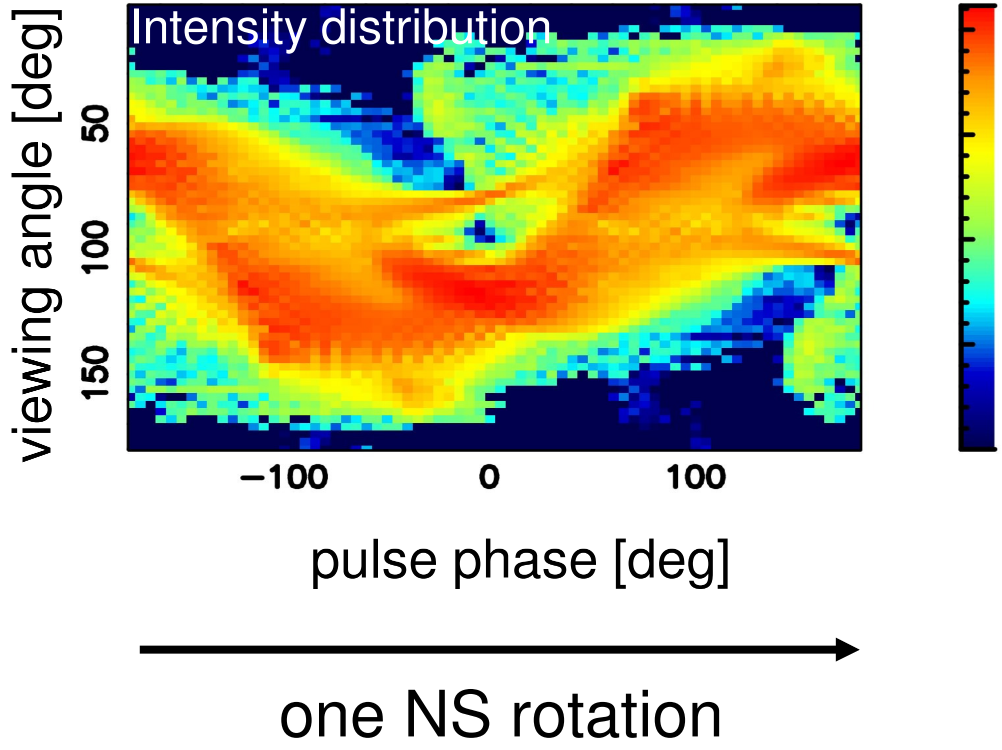

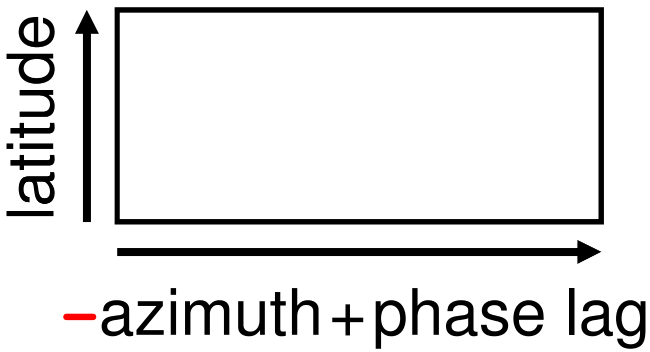

Photons emitted at smaller azimuth arrives earlier.

§5 New gap theory: Self-consistent approach

Photons are emitted along the local ***B*** field lines (in the co-rotating frame) by relativistic beaming and propagate in a hollow cone.

The hollow cone emission is projected on the 2-D propagation directional plane.

If we specify the observer's viewing angle, we obtain the pulse profile.

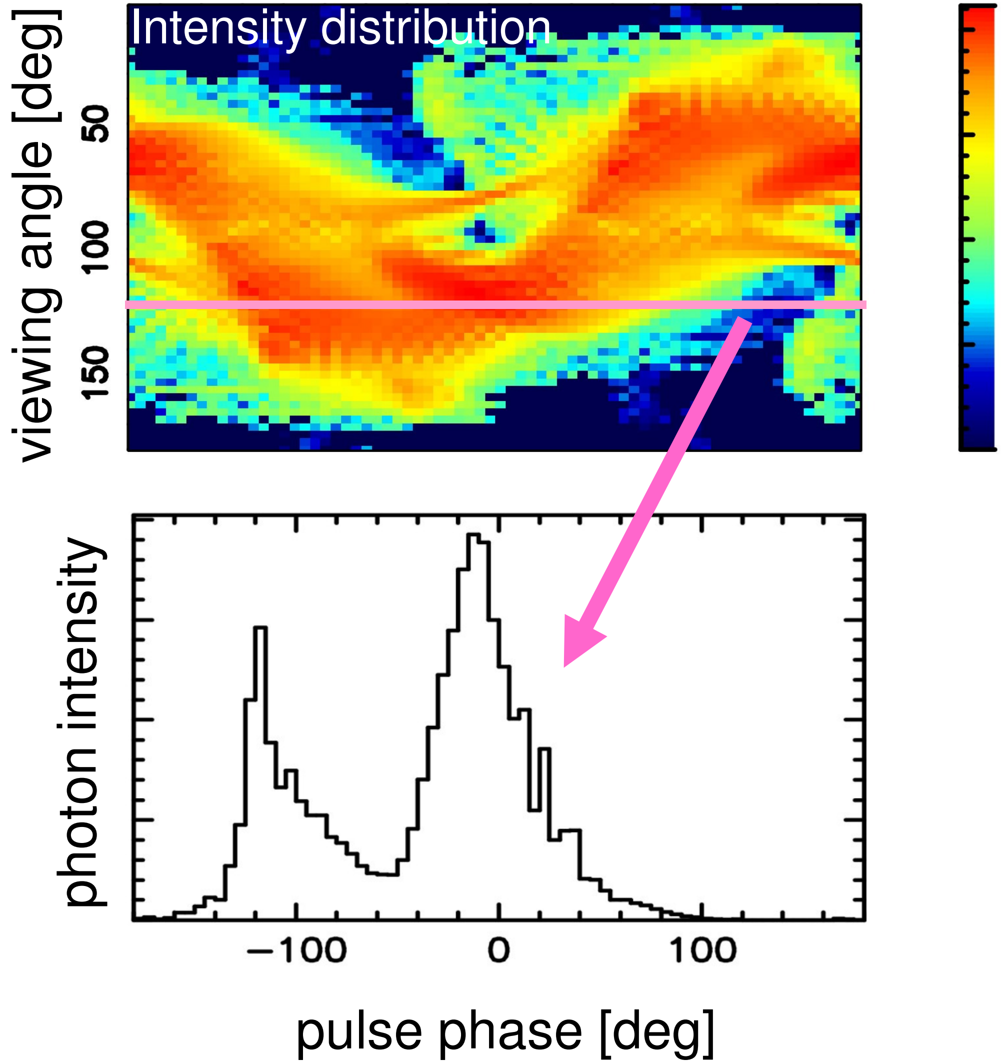

§5 New gap theory: Self-consistent approach

Predicted spectra reproduce observations, if we assume appropriate viewing angle (e.g., ~100°).

Fig.) OG prediction of Crab νF_ν spectra

solid:
un-abs. primary

dashed:
un-abs. 2ndary

red:
to be observed,
prim.+2nd+3rd

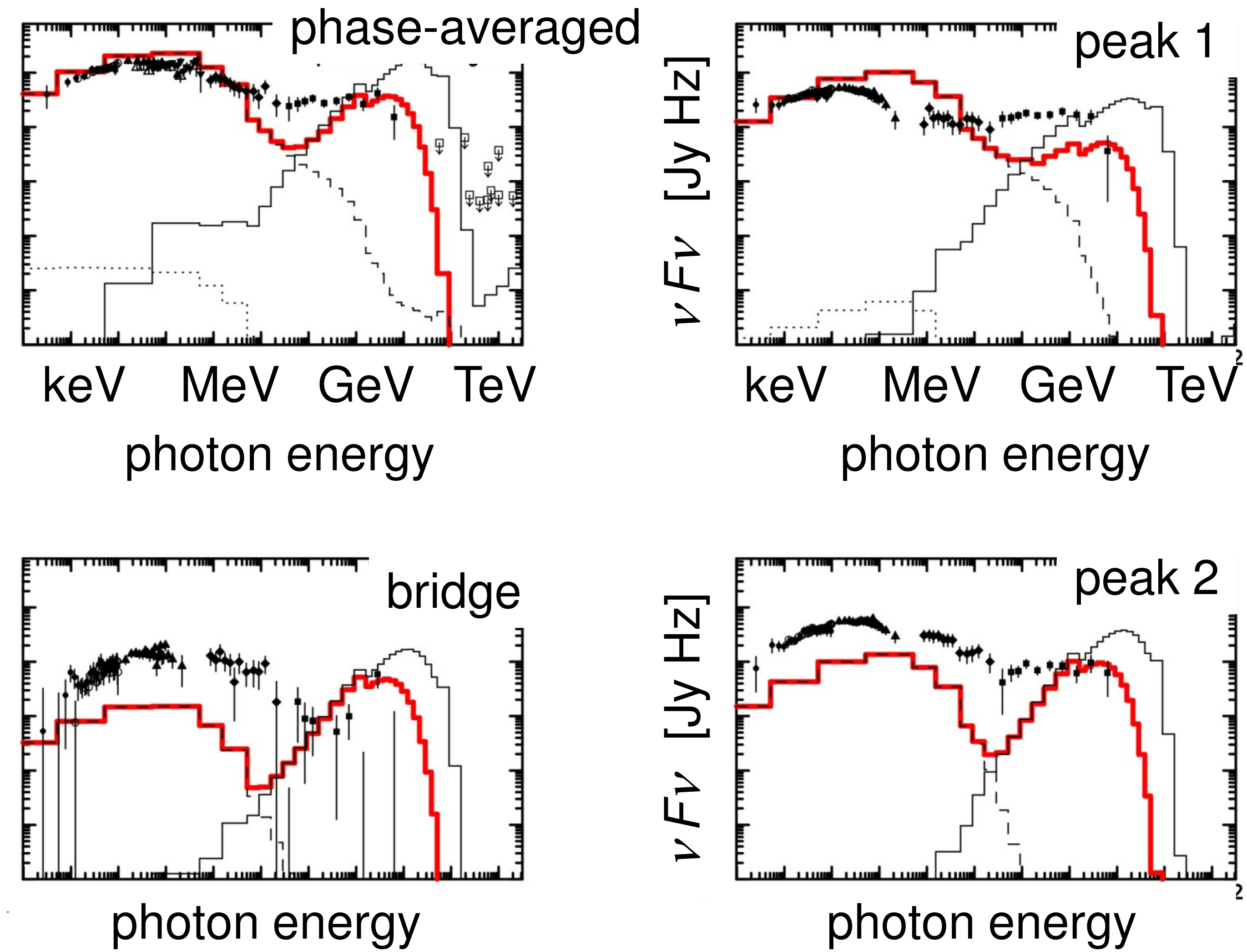

Summary

- High-energy emissions from pulsar magnetospheres are first solved from the set of Maxwell (div$\boldsymbol{E}=4\pi\rho$ only) and Boltzmann eqs., if we specify P, dP/dt, α_{incl}, kT_{NS}. We no longer have to assume the gap geometry, $E_{\parallel}$, $e^{\pm}$ distribution functions. ($\boldsymbol{B}$ field $\leftarrow$ vacuum rotating dipole solution)

- The obtained solution for the Crab pulsar corresponds to a quantitative extension of the previous, phenomenological OG models, and qualitatively reproduces the observations in IR-VHE.

- SG model can account for less than 10% of the observed Crab γ-ray flux.

- The same scheme can be applied for arbitrary rotation-powered pulsars.

§1 Introduction: The γ-ray sky

The *Large Area Telescope* (20 MeV – 300 GeV) aboard the *Fermi Gamma-Ray Space Telescope*.

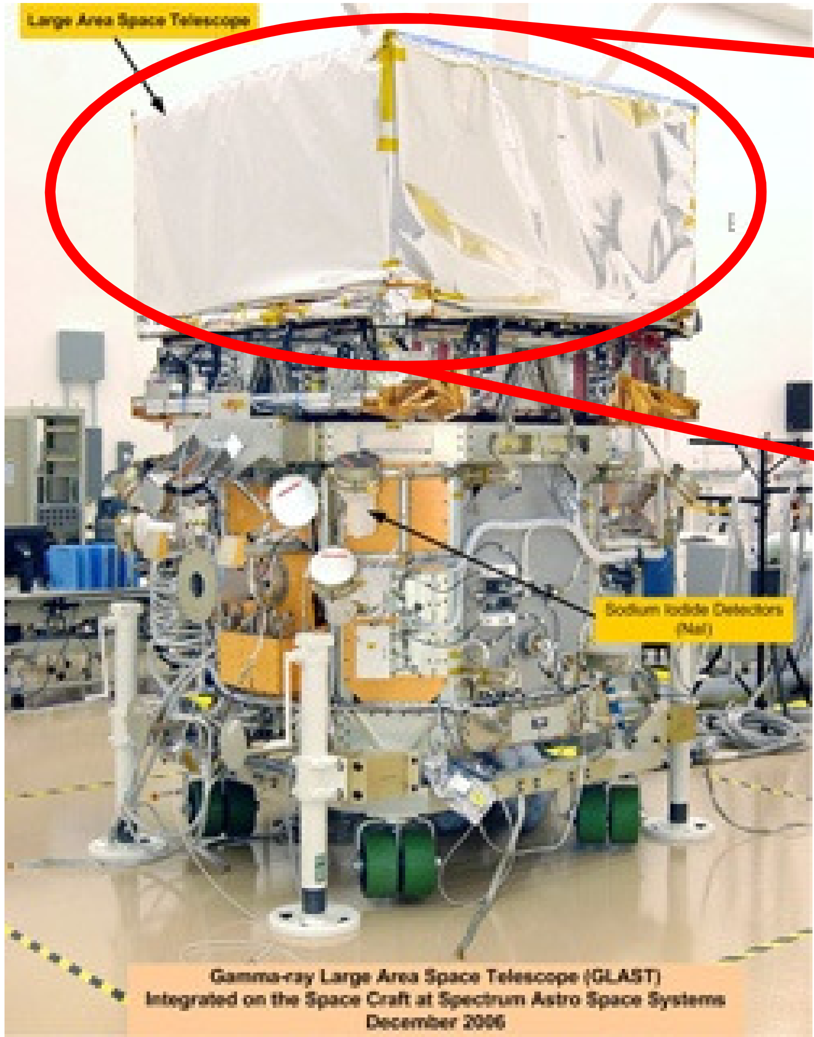

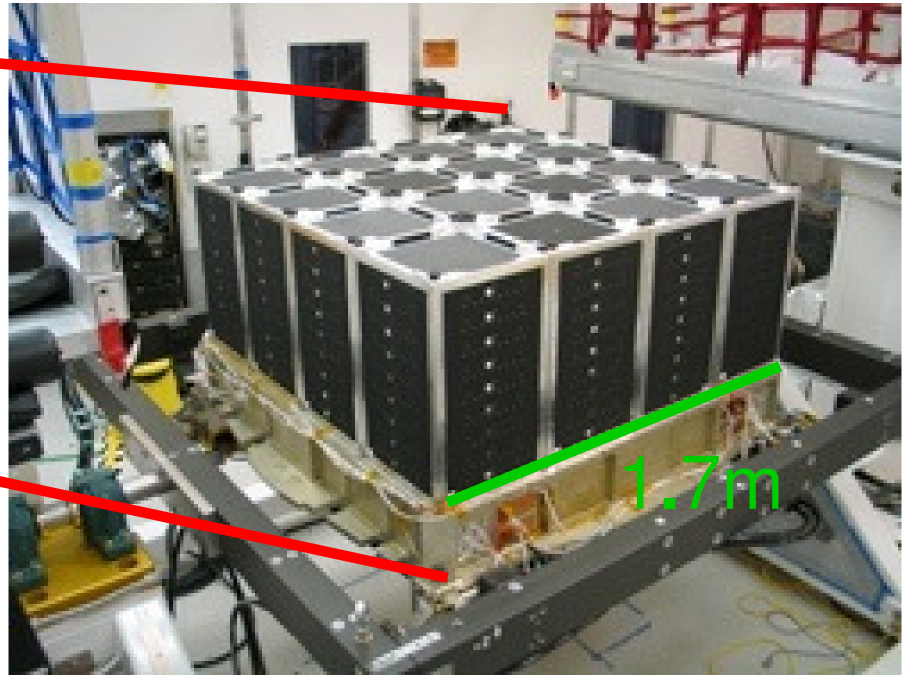

LAT PSF ~ 0.1° @ 1 GeV
FOV ~ 2.5 ster
sensitivity ~ 30*EGRET

§1 Introduction: The γ-ray sky

The *Large Area Telescope* (20 MeV – 300 GeV) aboard the *Fermi Gamma-Ray Space Telescope*.

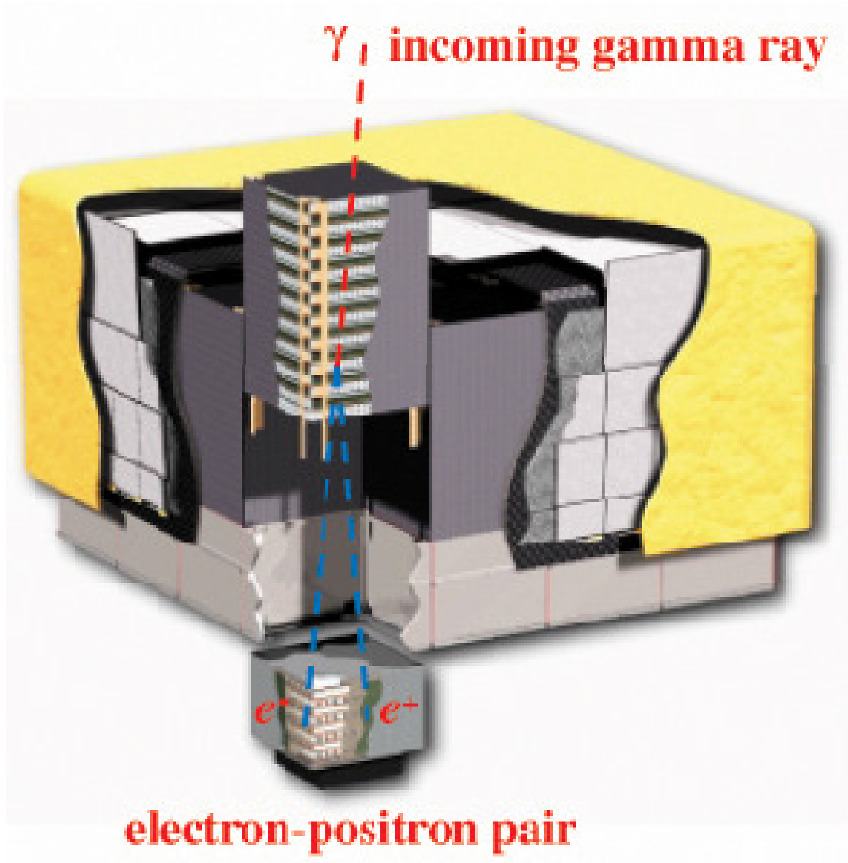

§1 Introduction: CGRO observations

γ-ray pulsars emit radiation in a wide frequency range:

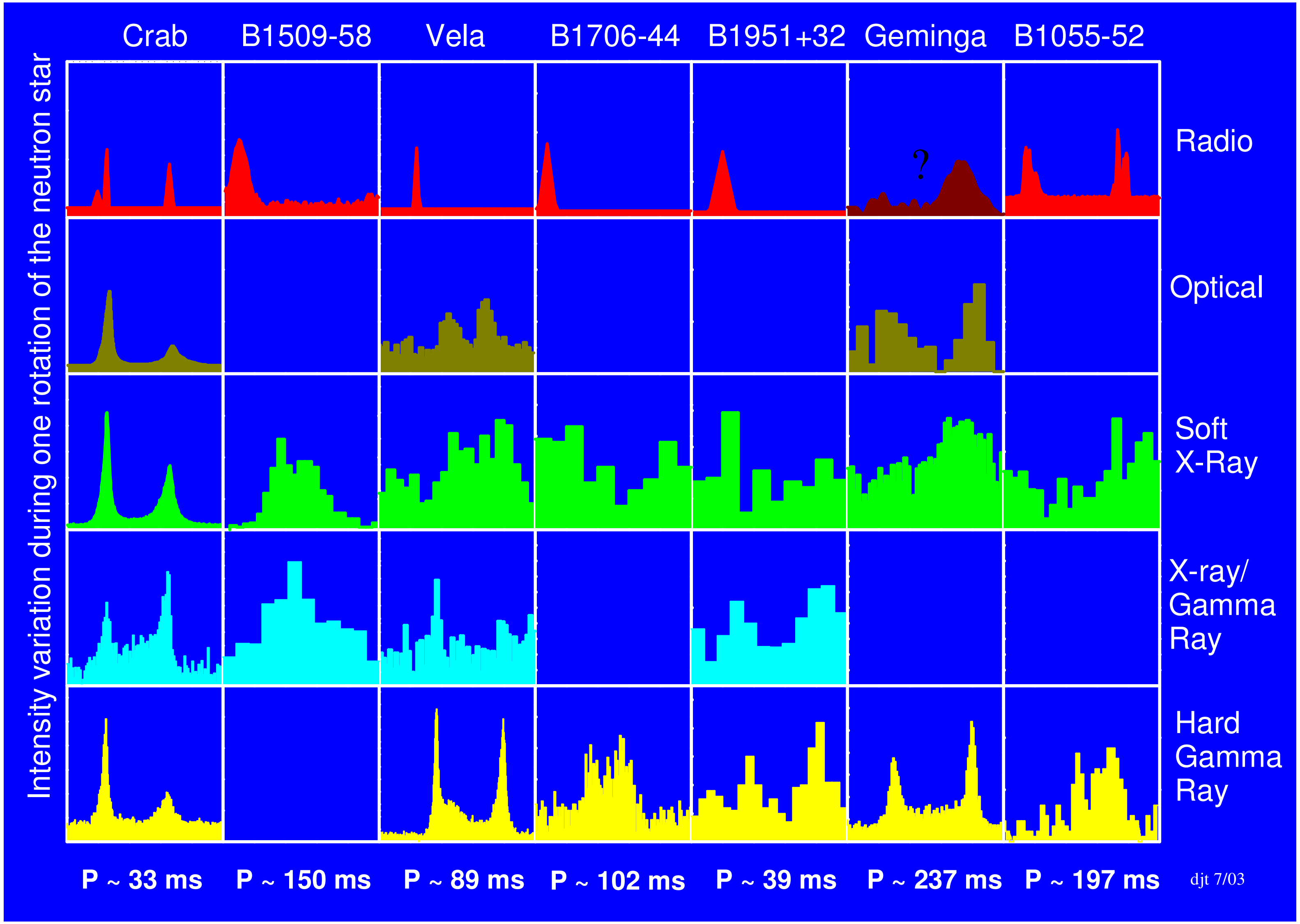

Thompson 2003, astro-ph/0312272